Cyclin CLB2 mRNA localization determines efficient protein synthesis to orchestrate bud growth and cell cycle progression

Evelina Tutucci[1,2,*], Anna Maekiniemi[1], Jacky L. Snoep[3,4], Markus Seiler[5], Kelly van Rossum[2], David D. van Niekerk[3], Philipp Savakis[2], Kathi Zarnack[5] and Robert H. Singer[1,6,*]

Affiliations:

[1] Anatomy and Structural Biology, Albert Einstein College of Medicine, 1300 Morris Park Avenue, 10461 Bronx, NY, USA

[2] Systems Biology Lab Amsterdam Institute of Molecular and Life Sciences (AIMMS), Vrije Universiteit Amsterdam, Amsterdam, The Netherlands

[3] Department of Biochemistry, University of Stellenbosch, Private Bag X1, Matieland, 7602, South Africa

[4] Department of Molecular Cell Physiology, VU University Amsterdam, De Boelelaan 1085, 1081 HV, Amsterdam, The Netherlands

[5] Buchmann Institute for Molecular Life Sciences (BMLS) & Faculty of Biological Sciences, Goethe University Frankfurt, Max-von-Laue-Str. 15, 60438 Frankfurt, Germany

[6] Janelia Research Campus of the HHMI, Ashburn, USA

*Co-corresponding authors: Evelina Tutucci evelina.tutucci@vu.nl and Robert H. Singer robert.singer@einsteinmed.org

Keywords: mRNA localization, localized translation, smFISH, MS2 system, ZIP-code, cell cycle, mitosis, *CLB2*, B-type cyclin, fluorescence microscopy

Abstract

mRNA localization to subcellular compartments has been reported across all kingdoms of life and it is generally believed to promote asymmetric protein synthesis and localization. In striking contrast to previous observations, we show that in *S. cerevisiae* the B-type cyclin *CLB2* mRNA is localized and translated in the yeast bud, while the Clb2 protein, a key regulator of mitosis progression, is concentrated in the mother nucleus. Using single-molecule RNA imaging in fixed (smFISH) and living cells (MS2 system), we show that the *CLB2* mRNA is transported to the yeast bud by the She2-She3 complex, via an mRNA ZIP-code situated in the coding sequence. In *CLB2* mRNA localization mutants, Clb2 protein synthesis in the bud is decreased resulting in changes in cell cycle distribution and genetic instability. Altogether, we propose that *CLB2* mRNA localization acts as a sensor for bud development to couple cell growth and cell cycle progression, revealing a novel function for mRNA localization.

Introduction

Over the past decades, RNA imaging technologies revealed that hundreds of mRNAs localize to various subcellular compartments, from bacteria to multicellular eukaryotic organisms, suggesting that mRNA trafficking is a conserved and integral part of gene expression regulation[1–7]. However, for many mRNAs, the physiological function of their localization remains uncertain.

Current studies suggest that the primary role of mRNA trafficking is to control asymmetric protein distribution to sustain local functions such as cell migration and polarity[5,8]. Even in the single-cell organism *S. cerevisiae*, dozens of mRNAs localize to the endoplasmic reticulum, mitochondria, and the growing bud[9]. The best-characterized localized mRNA is *ASH1*, which is transported to the yeast bud on actin filaments by the She2-She3 complex and the type V myosin motor Myo4[10–17]. The RNA binding proteins (RBP) Khd1 and Puf6 bind the *ASH1* mRNA and inhibit its translation until the bud-localized kinases Yck1 and CK2 phosphorylate Khd1 and Puf6 and thereby release the inhibition and allow local translation to occur[18–23]. The Ash1 protein is subsequently asymmetrically segregated into the daughter nucleus, where it controls the mating-type switching program[11,24,25]. An additional kinase-RBP pair, Cbk1-Ssd1, has been shown to localize to the bud[26] and tune the translation of specific mRNA targets[27–29]. The coordination between these translation regulators remains unclear.

Besides *ASH1*, multiple mRNAs have been found to interact with the She2-She3-Myo4 complex[30]. Among these mRNAs is *CLB2*, which encodes a conserved nuclear-localized B-type cyclin, interacting with and controlling the substrate specificity of the cyclin-dependent kinase Cdk1[31–41]. Clb2-Cdk1 regulates entry and progression throughout mitosis in a threshold-dependent manner[32,42–45], by phosphorylating transcriptional and post-transcriptional regulators[34,46,47]. This triggers a positive feedback loop leading to the transcription of the *CLB2* cluster[36,48–50], a set of 35 genes including *CLB2*, expressed during the G2/M phase transition[50]. Furthermore, Cdk1-Clb2 controls spindle pole bodies elongation and in turn chromosome segregation and genome stability[51,52]. Aberrant Clb2 expression -depletion or over-expression- results in abnormal mitotic

progression and cell size alteration[31,32,34,52]. To achieve accurate periodic Clb2 expression, cells combine cell-cycle-dependent mRNA synthesis[53,54], controlled mRNA decay[55], and proteasome-dependent protein degradation[56,57]. While the molecular events controlling *CLB2* transcription and protein degradation are well characterized, as well as Clb2 function during cell cycle progression, it remains unclear whether and how *CLB2* mRNA translation and Clb2 protein levels are modulated in response to changes in cell growth that require adaptation of cell cycle progression. To address this question, we combined single-molecule mRNA fluorescence *in situ* hybridization (smFISH)[58,59] and immunofluorescence (IF)[60–64] to simultaneously detect *CLB2* mRNA and its protein product in individual cells. Furthermore, to study dynamic gene expression changes in intact living cells[65,66], we utilized the MS2 system (MBSV6) optimized to endogenously tag unstable mRNAs in *S. cerevisiae*[67–69]. Our work shows that *CLB2* mRNAs are efficiently localized in the bud during the G2/M phase, while the Clb2 protein is localized to the mother nucleus. *CLB2* mRNAs are transported to the bud by the She2-She3 complex recognizing a single ZIP-code in the coding sequence necessary for localization. We find that the *CLB2* mRNA is preferentially translated in the bud, and that this localized translation does not require translation inhibition by Puf6, Khd1 or Ssd1 during transport. Consistent with these observations, lack of *CLB2* mRNA localization results in reduced Clb2 protein synthesis, leading to cell cycle and growth defects. Altogether, we propose that *CLB2* mRNA localization regulates protein synthesis and acts as a cellular timer to couple bud growth and cell cycle progression.

Results

CLB2 mRNAs localize in the bud from S phase to Mitosis

To precisely quantify *CLB2* mRNA expression throughout the *S. cerevisiae* cell cycle, we combined smFISH and IF[64,70,71]. To monitor cell cycle progression, nuclear localization of the transcription factor Whi5 was used to classify early G1 phase[72], while G2 and mitotic cells were identified by staining tubulin (Tub1) and monitoring microtubules stretching between the mother and the daughter mitotic spindles[73] (**Fig. 1a**). *CLB2* smFISH revealed that mRNAs are detected from late S phase, when the bud emerges from the mother cell, until the end of anaphase. Quantification of *CLB2* mRNA spots showed that *CLB2* mRNAs are found in 60.7% of cells in an unsynchronized population (**Fig. 1Sa**). The expression peak occurred during G2 (average 10.2 ± 5.7 mRNAs/cell) when about 50% of the cells showed an active transcription site (**Fig. 1b-c**) with on average 2.9 ± 1.5 nascent mRNAs per transcription site, similar to previous studies[55](**Fig. 1Sb**). Furthermore, in expressing cells, the *CLB2* gene showed Poissonian transcription kinetics typical of constitutive genes[74,75], suggesting that this cell-cycle regulated gene is likely transcribed in a single activation event with a fixed initiation rate. From late S phase until anaphase, we observed that *CLB2* mRNAs localize to the bud from the first stages of bud formation. Throughout the budded phases, we measured up to 65.6% of mRNA in the bud, as compared to the distribution of the control mRNA *MDN1,* where only 17.2% of mRNAs are found in the bud (**Fig. 1b, d, 1Sc-d**). *CLB2* mRNA bud localization is independent of the *S. cerevisiae* background since we observed it both in BY4741, used throughout this study, as well as in the W303 background (**Fig. 1Se**).

CLB2 mRNAs efficiently localize in the bud of living S. cerevisiae cells

To investigate *CLB2* mRNA localization dynamics in living cells, we used an MS2 system optimized for yeast mRNA tagging (MS2 binding sites V6, MBSV6)[67,68,76]. We inserted 24xMBSV6 in the 3' UTR of the endogenous *CLB2* locus (**Fig. 2Sa**). To confirm that mRNA tagging with

MBSV6 did not alter *CLB2* mRNA expression and degradation, unlike with previous MS2 variants[67,77,78], we performed two-color smFISH with probes targeting either the coding sequence (CDS) or the MBSV6 loops [67,68], to compare the expression of the endogenous and the tagged *CLB2* mRNA. This confirmed that MS2-tagged mRNAs are full-length and correctly localized in the bud (**Fig. 2Sb**). Furthermore, comparable mRNA levels were observed whether the mRNA was MS2-tagged, with or without GFP-tagged MS2 coat protein (MCP-GFP), which is used to detect mRNAs in living cells (**Fig. 2Sc-e**).

To monitor cell cycle progression and bud emergence in living cells, we endogenously tagged the bud neck protein Cdc10 with tdTomato in the *CLB2*-MS2-tagged strain (**Fig. 2a**). We performed time-lapse imaging every 2 minutes and measured *CLB2* mRNA expression throughout the cell cycle by acquiring z-stacks encompassing the cell volume (**Video 1**). To reduce perturbations in gene expression due to synchronization protocols[79,80], we quantified *CLB2* mRNA expression in unsynchronized cells, using the bud neck marker expression to compare cells. This revealed that up to 62.9% of *CLB2* mRNAs localized in the bud (**Fig. 2b-c**), consistent with the smFISH quantifications (**Fig. 1e**). Furthermore, mRNAs are degraded before the end of mitosis with a half-life of 3.8 ± 1.4 min, similar to previous measure performed for untagged *CLB2* mRNA[55], demonstrating that the MS2 system does not affect *CLB2* mRNA stability (**Fig. 2b-d; 2Sf**). Interestingly, imaging of mother-daughter pairs for more than one cell cycle showed that the daughter cell initiated *CLB2* mRNA expression about 20 minutes after the mother (**Fig. 2d**). This observation is consistent with previous evidence showing that *S. cerevisiae* daughter cells are born significantly smaller than mothers and that cell size control occurring during G1 regulates the entry into the next cell cycle[34,81,82]. High frame-rate imaging every 100 ms revealed that, as the bud grows, the number of *CLB2* mRNAs localized in the bud rapidly increases (**Fig 2e, Video 2**). Altogether, these results show that *CLB2* mRNAs are efficiently transported to the bud, consistent with previous measurements estimating directed mRNA transport velocity in eukaryotic cells to be about 1 μm/s[83], suggesting that *CLB2* mRNAs reach the bud within seconds (**Fig 2e**).

The She2-She3 complex independently transport the CLB2 and ASH1 mRNAs to the bud

To elucidate the function of *CLB2* mRNA localization, we first investigated *CLB2* mRNA transport. We performed smFISH-IF throughout the cell cycle for the *CLB2* mRNA in *SHE2* or *SHE3* gene deletion strains to test whether the She2-She3 complex, required for *ASH1* mRNA transport[10–17], is also involved in *CLB2* mRNA localization. This revealed that in *Δshe2* and *Δshe3* strains, localization is strongly affected (**Fig. 3a, 3Sa**). We also observed that during mitosis, when the bud reaches its maximum size, only up to 24.5% and 23.6% of *CLB2* mRNAs are found in the bud of the *Δshe2* and *Δshe3* strains, respectively (**Fig. 3Sb-c**). Even though the *CLB2* and *ASH1* mRNAs are transported by the same complex, we do not observe co-transport, possibly because *CLB2* expression peak precedes *ASH1* occurrence during late anaphase (**Fig. 3Sd-g** and **Online Methods**). Furthermore, we observed that *CLB2* mRNAs are mostly single-molecules (**Fig. 3Sh**), suggesting that *CLB2* and *ASH1* mRNAs are independently localized to the bud by the She2-She3 complex.

The CLB2 mRNA has a conserved ZIP-code in the coding sequence

As the She2-She3 complex is required for *CLB2* mRNA localization, we hypothesized that the *CLB2* mRNA might possess a ZIP-code akin to the *ASH1* ZIP-code. Previous work defined the sequence and structure of the *ASH1* mRNA ZIP-code bound by She2[13,84–86]. Based on sequence and structure similarity, a pattern search was performed to predict occurrences within the *CLB2* mRNA (see **Online Methods**). We identified one high-confidence site in the CDS at position 1111-1145 (**Fig. 3b-c**). To test the role of the predicted site, we generated a *CLB2* synonymized mutant whereby the CDS was mutagenized at nine bases to destroy the ZIP-code structure, while keeping the protein sequence and the codon optimization index unaltered (*ZIP mut*, **Fig. 3d**). A pattern search confirmed that the ZIP-code was destroyed upon synonymization. smFISH revealed that the *CLB2* mRNA bud localization was lost in the *CLB2* ZIP-code mutant (**Fig. 3e**). This was further confirmed by quantifying the *CLB2* mRNA bud-mother distribution (**Fig. 3f**),

thereby demonstrating that the ZIP-code in the CDS of the *CLB2* mRNA is sufficient to control bud mRNA localization, possibly by recruiting the She proteins. To further characterize *CLB2* mRNA localization, we quantified the mRNA peripheral distribution index (PDI) in budded cells using the RNA Distribution Index Calculator[87] (see **Online Methods**). The PDI measures the location of the mRNA in relation to the nucleus and it allows to compare the localization of multiple mRNA species. An index value equals 1 for diffusely distributed mRNAs or >1 if the mRNA has a polarized pattern[87,88] (**Fig 3g**). This analysis revealed a PDI of 1.9 ± 0.42 for the *CLB2* mRNA, similar to the index value of the control mRNA *ASH1* (PDI = 2.2 ± 0.43) (**Fig 3h**). The PDI value was significantly reduced for *CLB2* in the *Δshe2* (PDI = 0.5 ± 0.2), *Δshe3* (PDI = 0.4 ± 0.13) and *CLB2* ZIP-code mutant strain (PDI = 0.5 ± 0.16) (ANOVA statistical test: $F(4, 185) = 15.74$, $p < 0.0001$), with PDI values similar to the non-localized mRNA *MDN1* (PDI = 0.6 ± 0.18) (**Fig. 3h, 1Sb**). Thus, the She2-3 complex is required to transport *CLB2* mRNAs to the bud via a conserved ZIP-code sequence.

Lack of CLB2 mRNA localization affects Clb2 protein expression

To elucidate whether *CLB2* mRNA localization influences its expression, we measured *CLB2* mRNA and protein levels in the localization mutants. Using smFISH, we found no significant difference in the number of mature or nascent RNAs in the *Δshe2*, *Δshe3,* or *CLB2* ZIP-code mutant strains compared to WT cells (**Fig. 4a-b**). Conversely, a western blot of the endogenously modified myc-tagged Clb2 protein showed that the protein expression in Δ*she2* or Δ*she3* and, even more, in the *CLB2* ZIP-code mutant was strongly reduced compared to WT cells (**Fig. 4c-d, 4Sa**). To test whether the decrease in protein expression was due to a change in protein degradation, we performed stability assays by treating WT and localization mutants with the translation inhibitor cycloheximide and measured the protein abundance over time (**Fig. 4e-f, 4Sb-c**). No significant difference was observed in the stability of the localization mutants

compared to WT cells, suggesting that *CLB2* mRNA localization controls Clb2 protein synthesis, rather than the stability of *CLB2* mRNA or protein.

Lack of CLB2 mRNA localization does not affect Clb2 protein localization

Next, we investigated whether mRNA localization affected Clb2 protein localization. To this end, *CLB2* was endogenously tagged with yeast optimized GFP (yeGFP[89]) in WT and *CLB2* mRNA localization mutants. We observed that Clb2 is predominantly found in the nucleus in WT and mRNA localization mutants (**Fig. 4g**), as previously reported[38,39,41]. Consistent with the western blot results (**Fig. 4c-d**), the fluorescence of the *CLB2* ZIP-code mutant was below detection level by live imaging (**Fig. 4g**). Furthermore, comparing Clb2 expression during a complete cell cycle in living WT and Δ*she2* cells (**Fig. 4Sd-e**), revealed that in contrast to WT cells, where a rapid Clb2 increase proportional to bud growth is observed, in Δ*she2* cells a slower protein accumulation was measured, accounting for the decrease in Clb2 expression. In addition, Clb2 was observed in the mother nucleus already during the G2 phase (**Fig. 4g**, top panels), when the mRNAs are already localized to the bud (**Fig. 1b, 2b, 3a**). Altogether, these results suggest that *CLB2* mRNA localization is not used to segregate the Clb2 protein in the daughter cell, as instead is observed for Ash1[11,24,25], but rather to control *CLB2* mRNA translation efficiency in the bud before the protein is imported back to the mother nucleus.

CLB2 mRNAs and protein co-localization suggests preferential translation in the bud.

To detect *CLB2* mRNAs and their site of translation in single cells, we generated a yeast strain where 25 Myc tags were inserted at the N-terminus of the *CLB2* endogenous gene (**Fig. 5Sa-b**). This amplification strategy increases the fluorescent signal of Clb2 proteins without affecting the strain growth (**Fig. 4Sa**). Next, we combined smFISH and IF to simultaneously detect *CLB2* mRNAs and proteins in fixed cells. In addition, IF against tubulin was used to score the cell cycle phases. This approach revealed that the bulk of Clb2 proteins accumulated in the mother (M) nucleus from G2 to mitosis (**Fig. 5a-b**), while the mRNA was preferentially found in the bud (B)

(**Fig. 5a, c**), suggesting that Clb2 proteins were efficiently imported back to the mother nucleus, as observed by live imaging (**Fig. 4g**), and as shown previously[38–41]. Interestingly, from G2 to mitosis, Clb2 protein foci were also found in the bud in close proximity of *CLB2* mRNAs, suggesting that these foci may represent the site of mRNA translation (**Fig. 5a**, yellow arrowheads). Quantification of co-localized single mRNAs and protein foci within 250 nm distance (i.e. the resolution of our system), revealed that in WT cells, more mRNA-protein foci were found in the bud, while in the localization mutant *Δshe2*, mRNA-protein foci are preferentially found in the mother cell where the bulk of mRNAs is localized (**Fig. 5d-e**, **Fig. 3a**). Furthermore, we found a reduction of the percentage of bud-localized mRNAs co-localized with protein foci in *Δshe2* cells compared to WT cells (**Fig. 5f**), suggesting that in localization mutants *CLB2* mRNA translation efficiency may be reduced. This analysis could not be performed with the *CLB2* ZIP-code mutant because the protein signal was too weak (**Fig. 4g**). It is interesting to note that even in WT cells, only about 25% of the bud-localized mRNAs are found in close proximity to protein foci (**Fig. 5f**), suggesting that *CLB2* mRNAs are poorly translated, as previously reported[90].

Finally, we quantified the accumulation of mRNA-protein foci in WT cells exposed for a short period of time to the translation elongation inhibitor cycloheximide (CHX, 20 minutes at 100 µg/ml). This revealed that translation inhibition leads to an increase in *CLB2* mRNA levels accompanied by an accumulation of mRNAs in the mother cell (**Fig. 5Sc-e**). Furthermore, we observed a reduction of the Clb2 protein foci in the bud (**Fig. 5Sf**), compared to control conditions (**Fig. 5b**), consistent with a decrease in protein synthesis. Furthermore, the increased amount of *CLB2* mRNAs found in the mother upon CHX treatment suggested that mRNA translation may play a role in the asymmetric distribution of *CLB2* mRNAs in the bud, possibly by slowing down the diffusion kinetics of mRNAs bound to ribosomes, as previously shown in mammalian cells[61,91,92]. To test this hypothesis, we simulated the distribution of *CLB2* mRNAs upon their localization in the bud of a G2 cell, with bud and mother volumes based on our measurements. We included measured *CLB2* mRNA decay rates and assumed an apparent mRNA diffusion

coefficient based on previously reported measurements performed in eukaryotic cells[91] (see **Online Methods**). A fast coefficient of 0.4 $\mu m^2/s$ was previously measured for non-translated mRNAs, and a slower coefficient of 0.1 $\mu m^2/s$ was measured for translated mRNAs[91]. Interestingly, our model suggests that if we assume either a slow or a fast apparent mRNA diffusion coefficient of 0.1 $\mu m^2/s$ or 0.4 $\mu m^2/s$, respectively, we do not obtain the expected enrichment of the *CLB2* mRNA in the bud (**Fig. 5Sg-h**). To predict the accumulation of about 65% of the mRNA in the bud observed during the G2 phase, we need to include in the simulation the presence of a high-affinity anchoring factor promoting *CLB2* mRNA segregation in the bud (**Fig. 5Si**). Altogether, these data suggest that in WT cells, *CLB2* mRNAs are preferentially translated in the bud where the mRNA is actively transported and localized via an unknown anchoring mechanism, which may include the association with ribosomes and other yet unidentified factors. Furthermore, both in *Δshe2* cells and in translationally repressed cells (CHX), we observed an increase of protein foci in the mother cell (**Fig. 5d, 5Sf**), despite protein levels being decrease under these conditions (**Fig. 4c, 4e-f**), suggesting that translation in the mother cell may be less efficient, resulting in reduced Clb2 protein levels in the localization mutants.

Clb2 protein expression is not affected by the translation regulators Puf6, Ssd1 and Khd1

To investigate whether *CLB2* mRNAs are preferentially translated in the bud as a result of translation repression prior to localization, we tested if the RNA binding proteins Puf6[18,19,23], Khd1[20–22] and Ssd1[27–29], previously shown to inhibit translation of bud-localized mRNAs, influenced Clb2 protein levels. We performed a western blot of Myc-Clb2 in strains lacking *SSD1, KHD1* or *PUF6* genes, to investigate whether an increase in Clb2 protein could be observed (**Fig. 6a**). This revealed no significant difference in protein levels between the WT and the mutant strains (ANOVA statistical test: $F(3, 8) = 0.7677$, $p = 0.3$; **Fig. 6b**). Furthermore, we analyzed by smFISH whether *CLB2* mRNA localization or abundance were affected in *Δssd1, Δkhd1* or *Δpuf6* strains. This showed that the *CLB2* mRNAs are still localized in the bud, suggesting that these RBPs are not required for transport nor bud localization (**Fig. 6c**). Interestingly, we found a

significant increase of *CLB2* mRNA counts in the Δ*puf6* strain compared to WT (6.86 ± 1.23 and 4.27 ± 0.52 mRNA/cell, respectively, p<0.0001) (**Fig. 6d, 6Sa**). This rise was not caused by an increased RNA synthesis, measured by the number of nascent RNAs per transcription site (**Fig. 6e**), but by a 25% increase in the number of cells with two active transcription sites (**Fig. 6Sb-c**). Since in WT haploid cells, we only observed one *CLB2* allele transcribed during the G2/M phase, when two copies of the gene are present, this indicated that Puf6 may regulate *CLB2* gene dosage by repressing the transcription of *CLB2* second allele. Altogether, these results suggest that *CLB2* mRNAs are not translationally repressed by factors controlling *ASH1* mRNA expression. While it is possible that other, yet unidentified factors exist, our data suggest the possibility that *CLB2* mRNA may be translated outside of the bud, albeit at a reduced rate.

CLB2 mRNA localization mutants display cell cycle progression defects

Our results so far indicated that the yeast bud promotes *CLB2* mRNA translation and a rapid increase of Clb2 protein levels proportional to bud growth (**Fig. 4c-d, 4Sb**). This suggested that *CLB2* mRNA localization may act as a cellular signal reporting on bud growth to the mother nucleus and coordinating cell growth and division. To test whether the decrease of Clb2 protein levels observed in *CLB2* mRNA localization mutants affected cell cycle progression and growth, we performed growth assays under different nutrient availabilities. In rich media (Synthetic complete medium with 2% glucose), the *CLB2* ZIP-code mutant clones did not show a growth defective phenotype. However, in the presence of a limiting carbon source (Synthetic complete medium with 0.1% glucose), it became apparent that the *CLB2* ZIP code mutant showed varying growth phenotypes with a marked clonal variability (**Fig. 7a**), suggesting incomplete phenotypic penetrance of the mutation. We proceeded with the analysis of three independently isolated clones (*ZIP cl1*, *ZIP cl2*, *ZIP cl3*).

We first tested by spot assay whether the localization mutants showed a growth defect at different temperatures (26°C, 30°C, 37°C) and growth limiting conditions set by the presence of different carbon sources (0.1% glucose or 2% glycerol/ethanol compared to 2% glucose). While the She

mutants grew like the WT strain, the ZIP-code mutants showed a clone-dependent growth defect, with the *ZIP cl1* showing reduced growth in carbon-limiting conditions when compared to the other clones and WT cells (**Fig. 7b**). Dynamic growth measurements of cells transitioned from rich liquid media to either liquid media containing 0.1% glucose or 2% glycerol/ethanol (**Fig. 7c**), demonstrated a complete growth arrest for *ZIP cl1,* while the other ZIP clones (**Fig. 7c**) and the She mutants (**Fig. 7Sa**) did not show reduced growth.

Finally, to evaluate the impact of the ZIP-code mutation on cell cycle progression, we performed a cell cycle distribution analysis by DNA staining with Sytox Orange coupled with flow cytometry (see **Online Methods**). Analysis of cells grown in rich media revealed a reduction of the G2/M population for *ZIP cl2*, *ZIP cl3*, but not *ZIP cl1* compared to the WT cells (**Fig. 7d**), suggesting that in rich conditions, even when growth was not affected for the ZIP-code mutants, the distribution of cell through the cell cycle was altered. Furthermore, cell cycle analysis of cells grown for 20 hours in presence of 0.1% glucose or 2% glycerol/ethanol, revealed that all the ZIP-code clones behaved differently from WT cells, mostly displaying a G2/M phase delay, demonstrated by a relative increase in the number of cells in this phase (**Fig. 7e-f**). On the other hand, *ZIP cl1* grown on 2% glycerol/ethanol displayed an arrest in G1 (**Fig. 7f**) and an increase in cell size (**Fig. 7Sb**), consistent with the growth defect observed both on agar plates and in liquid cultures (**Fig. 7b-c**). Thus, the ZIP-code mutants demonstrated complex clonal phenotypes, possibly triggered by critically low Clb2 protein levels. In most of the cases, the ZIP-code mutants behaved like *ZIP cl2* and *cl3*, and displayed altered cell cycle distribution but not a growth defect, possibly due to compensatory effects played by G1 growth checkpoints[34,93]. However, at least three clones were independently isolated behaving like *ZIP cl1,* suggesting that critically low levels of Clb2 may trigger the accumulation of secondary mutations and a loss of coordination between cell cycle and cell size control. To test this hypothesis, we investigated whether the *ZIP cl1* could be rescued by the presence of a WT copy of the *CLB2* gene. To this end, we generated diploid

strains where the WT or the *ZIP cl1* mutant were crossed with a WT strain (**Fig. 7Sc**). Liquid growth in presence of 0.1% glucose or 2% glycerol/ethanol revealed a growth rescue for *ZIP cl1.* Altogether, our data suggest that in growth-limiting conditions, when bud growth is slowed down by the presence of suboptimal nutrients and in turn ribosomes and other key metabolites may be limiting in this compartment, *CLB2* mRNA localization and protein transport back to the nucleus may act as a biochemical signal adjusting the cell cycle in response to cell growth changes.

Discussion

Numerous instances in prokaryotic and eukaryotic organisms revealed that subcellular localization of mRNAs regulates the synthesis and asymmetric localization of proteins[8]. Here, we show that the B-type cyclin *CLB2* mRNA is efficiently localized to the yeast bud in a cell cycle-dependent manner, while the Clb2 protein is imported back to the mother nucleus, demonstrating the first example of mRNA and protein localization uncoupling. We characterized a new function for mRNA localization, which is to coordinate cell growth and cell cycle progression, possibly by sensing the bud translation capacity via the transport and local translation of the *CLB2* mRNA. We propose that by shuttling back to the mother nucleus, Clb2 signals to the mother cell when the bud is ready for mitosis, establishing a biochemical-based communication between distinct subcellular compartments.

Here, we combined single molecule RNA FISH-IF in fixed cells and a yeast-optimized MS2 tagging system for single RNA visualization in living cells to quantify, for the first time, the complete lifecycle of the *CLB2* mRNA and its protein product in intact cells. This approach revealed that *CLB2* mRNAs are transported to the bud as soon as this compartment is formed during late S phase (**Fig. 1,2,3**). Interestingly, previous reports showed that the B-type cyclin B1 is also asymmetrically localized in higher eukaryotes such as in the *Xenopus*[94] and *Zebrafish*[95,96] oocytes as well as in *Drosophila* embryos[1], suggesting that the spatiotemporal regulation of Clb2 expression is a conserved mechanism.

The She2-She3 complex, previously shown to localize other mRNAs such as *ASH1*[10–17], *IST2, TCB2, and TCB3*[12,30], is also required to localize *CLB2* mRNAs to the bud (**Fig. 3**). Furthermore, by combining imaging and modelling, we suggested that the efficient asymmetric localization of *CLB2* mRNAs is likely produced by a combination of active transport and bud anchoring via yet unknown RBPs (**Fig. 5S**). To elucidate the function of *CLB2* mRNA localization we identified the cis-acting element required for transport. A single RNA ZIP-code in the mRNA CDS is sufficient to ensure localization in the bud (**Fig. 3**). This ZIP-code has a sequence and predicted structure similar to the *ASH1* ZIP-code, supporting the notion that cis-elements bound by the She2 RBP are conserved[25,30,84]. Mutation of the ZIP-code RNA sequence caused an mRNA localization defect and correlated with a strong decrease in Clb2 protein expression (**Fig. 4**). Simultaneous visualization of the *CLB2* mRNA and proteins in fixed cells using the myc-tag reporter suggested that *CLB2* mRNAs are preferentially translated in the bud (**Fig. 5**). While this compartment promotes *CLB2* mRNA translation, we could not demonstrate that known mRNA translation inhibitors such as Puf6, Ssd1 and Khd1, prevent *CLB2* mRNA translation prior localization (**Fig. 6**). Unlike the Ash1 protein, the Clb2 protein is not restricted in the bud, possibly explaining why *CLB2* may not require translation inhibition. Yet unidentified translation inhibitors may also be involved in this process.

Interestingly, the *CLB2* ZIP-code mutant showed a further reduction in protein expression compared to the single SHE mutants, even though mRNA localization was equally impaired (**Fig. 4**). This suggested that the destruction of the ZIP-code may prevent not only the binding of the She proteins required for transport, but also the recruitment of translation factors that may travel together with the mRNA to the bud. Further investigations will be focused on identifying factors involved in controlling *CLB2* mRNA local translation.

We found that before the nucleus is divided during yeast closed mitosis, most of the Clb2 protein is efficiently imported back to the mother nucleus (**Fig. 4**), consistent with previous reports[38–41]. The best characterized function of Clb2 is to trigger mitotic entry via the phosphorylation of key

targets controlling transcription of mitotic genes, including *CLB2* itself, and spindle pole bodies formation. In line with these observations, *CLB2* deletion mutants have been shown to be defective in DNA repair, genome stability and cell size control[31,32,52]. Consistently, *CLB2* ZIP-code mutants display phenotypes including altered cell cycle distribution, the inability to grow under suboptimal nutrient conditions combined with changes in cell size. The strong clonal variability observed in our study also suggests that critical low levels of Clb2 may trigger genome instability and secondary mutations. Previous work showed that, when overexpressed[38,39] or when nuclear import is blocked[41], Clb2 can be found also at the bud neck. In our experimental settings, both in living and fixed cells and without overexpression, we did not observe Clb2 at this site. Nevertheless, we cannot exclude that a transient localization of Clb2 at the bud neck may have spatially-defined functions that may contribute to the observed phenotypes.

Altogether, our results suggest that *CLB2* mRNA localization in the bud regulates Clb2 protein synthesis to ensure coupling between cellular growth and cell cycle. An elegant mathematical model previously predicted a similar outcome, and suggested that *CLB2* mRNA localization may act as a bud sizer during the G2/M phase checkpoint[97]. Even though we did not observe specific bud size defects in the *CLB2* localization mutants, future studies may elucidate the role of *CLB2* localization during yeast cell size and cell cycle coordination. Thanks to improved imaging technologies and the advent of spatial transcriptomic, thousands of localized mRNAs have been identified in many model organisms[4]. We predict that additional functions for mRNA localization will emerge, revealing the importance of this process in controlling the spatiotemporal synthesis of proteins, from single-cell to multicellular organisms.

Acknowledgments

We thank X. Meng for help with cloning; W. Li, C. Eliscovich and S. Das for discussion and A. Gerber for discussion and critical reading of the manuscript. This work was supported by NIH grant GM57071 to R.H.S. E.T. was supported by Swiss National Science Foundation Fellowships P2GEP3_155692 and P300PA_164717, as well as by the Systems Biology lab at the Vrije Universiteit Amsterdam. We acknowledge financial support from the Department of Science and Technology/National Research Foundation in South Africa, (grant NRF-SARCHI-82813 to J.L.S.) and for grant 116298 (to D.D.v.N.). K.Z. was supported by the Deutsche Forschungsgemeinschaft (DFG) via the Research Unit FOR2333 (ZA 881/3-1).

Online methods

Yeast strains construction

Yeast strains were constructed in the BY4741 background as detailed in[68]. All strains where a gene of interest was tagged with MBSs in the 3'-UTR right after the STOP codon, were prepared as follow: PCR amplification of the MBS insert (see plasmids in Resource Table) followed by the kanamycin resistance gene, flanked by LoxP sequences, was performed with oligos (see Resource Table) containing homology sequences (70 nt) for the specific gene. For all strains, the Kanamycin resistance gene was removed by expressing the CRE recombinase under the control of the *GAL1* promoter (Resource Table, plasmids). Genomic DNA was extracted using standard techniques and PCR amplification of the 3'-UTR was loaded on a gel and sent for sequencing to verify the size and the sequence of the insert.

Plasmids construction

The synonymized *CLB2* region was synthesized as a DNA fragment by Genescript® with restriction endonuclease sites BglII and ClaI restriction sites. This fragment was used to replace the *CLB2* WT sequence in a plasmid encoding the *CLB2* promoter, CDS and UTRs. The promoter was preceded by the *URA3* marker flanked by LoxP sites, which were used to remove the marker upon integration into the yeast genome (pET531). 70-100 nucleotides *CLB2* homology sequences for insertion into the genome were cloned as well in the vector. Insertion of 5-Myc (synonymized multimer) or 25-Myc tags in the *CLB2* coding sequence was performed by restriction digestion into the BamHI site placed after the ATG codon.

Yeast cell cultures

All strains described are derived either by the *S. cerevisiae* background BY4741 (MATa; his3Δ1; leu2Δ0; met15Δ0; ura3Δ0) or W303 (MATa; ura3-1; trp1Δ 2; leu2-3,112; his3-11,15; ade2-1; can1-100). Strains are listed in the Resource Table. Yeast cultures were exponentially grown in 6.7 g/L Yeast Nitrogen Base medium (YNB) with 2% glucose and the appropriate amino acids to

complement auxotrophies (either Synthetic Complete (SC), or Drop-Out (DO) media). Cells were grown at the indicated temperature using constant shaking at 210 rpm. For spot-test experiments (Fig. 7), cells were grown overnight in SC or DO media with 2% glucose (see figure legends). In the morning cells were diluted to an OD_{600} of 0.8. Five ten-fold dilutions in water were prepared for each strains. 7 µL were spotted for each dilution on the indicated agar plates (20 g/L agar in the specific medium). For smFISH and live imaging, the details of the cell cultures are described in the Method sections below.

smFISH probes design

CLB2 probes were designed using the Stellaris™ Probe Designer by LGC Biosearch Technologies and purchased from Biosearch Technologies. *ASH1, MDN1* and *MBSV6* probes design was previously described in[67,68]. Probes sequence and fluorophores are provided in the Resource Table.

Single molecule fluorescence in situ hybridization (smFISH)

Single-molecule FISH (smFISH) was performed as follows. Yeast strains were grown overnight at 26°C in synthetic medium with 2% glucose and containing the appropriate amino acids to complement the strain auxotrophies. In the morning, cells were diluted to OD_{600} 0.1 and allowed to grow until OD_{600} 0.3-0.4. Cells were fixed by adding paraformaldehyde (32% solution, EM grade; Electron Microscopy Science #15714) to a final concentration of 4% and gently shaken at room temperature for 45 minutes. Cells were then washed three times with buffer B (1.2 M sorbitol and 100 mM potassium phosphate buffer pH=7.5) and resuspended in 500 µL of spheroplast buffer (buffer B containing 20 mM VRC (Ribonucleoside–vanadyl complex NEB #S1402S), and 25 U of Lyticase enzyme (Sigma #L2524) per OD of cells (~10^7 cells) for about 7-8 minutes at 30°C. Digested cells were washed once with buffer B and resuspended in 1 mL of buffer B. 150 µL of cells were seeded on 18 mm poly-L-lysine treated coverslips and incubated at 4°C for 30 minutes. Coverslips were washed once with buffer B, gently covered with ice-cold 70% ethanol

and stored at -20°C. For hybridization, coverslips were rehydrated by adding 2xSSC at room temperature twice for 5 minutes. Coverslips were pre-hybridized with a mix containing 10% formamide (ACROS organics #205821000)/2xSSC, at room temperature for 30 minutes. For each coverslip, the probe mix (to obtain a final concentration in the hybridization mix of 125 nM) was added to 5 µL of 10 mg/mL *E. coli* tRNA/ ssDNA (1:1) mix and dried with a speed-vac. The dried mix was resuspended in 25 µL of hybridization mix (10% formamide, 2×SSC, 1 mg/ml BSA, 10 mM VRC, 5 mM $NaHPO_4$ pH 7.5) and heated at 95°C for 3 minutes. Cells were then hybridized at 37°C for 3 hours in the dark. Upon hybridization, coverslips were washed twice with pre-hybridization mix for 30 minutes at 37°C, once with 0.1% Triton X-100 in 2xSSC for 10 minutes at room temperature, once with 1xSSC for 10 minutes at room temperature. Coverslips were mounted on glass slides using ProLong Gold antifade (4′,6-diamidino-2-phenylindole) DAPI to counterstain the nuclei (Thermofisher).

smFISH-IF

smFISH-IF was performed as previously described in[70,71]. In brief, smFISH-IF was performed in a similar way as smFISH, described above. After the last 1xPBS wash of the smFISH, IF was performed on the same coverslips. The smFISH was fixed in 4% PFA in PBS for 10 minutes at room temperature and then washed for 5 min at room temperature with 1x PBS. The coverslips were blocked with 1xPBS, 0.1% RNAse-free Bovine Serum Albumin for 30 minutes at room temperature before being incubated with primary antibodies (Thermofisher, mouse anti-tubulin, 1:1000; Sigma mouse monoclonal anti-Myc clone 9E10, 1:1000; Covance, mouse monoclonal anti-HA, 1:1000) in 1xPBS, 0.1% RNAse-free Bovine Serum Albumin for 45 minutes. After being washed with 1xPBS for 5 minutes at room temperature, the coverslips were incubated with the secondary antibody (goat anti-mouse Alexa 647 1:1500, or goat anti-mouse Alexa 488 1:1500) in 1xPBS, 0.1% RNAse-free Bovine Serum Albumin for 45 minutes at room temperature. Next, the coverslips were washed with 1x PBS three times for 5 minutes to remove excess antibody.

Coverslips were dehydrated by dipping them into 100% ethanol and letting them dry before being mounted onto glass slides using ProLong Gold antifade mounting solution with DAPI.

smFISH/ smFISH-IF image acquisition and analysis

Images were acquired using an Olympus BX63 wide-field epi-fluorescence microscope with a 100X/1.35NA UPlanApo objective. Samples were visualized using an X-Cite 120 PC lamp (EXFO) and the ORCA-R2 Digital CCD camera (Hamamatsu). Image pixel size: XY, 64.5 nm. Metamorph software (Molecular Devices) was used for acquisition. Z-sections were acquired at 200 nm intervals over an optical range of 8.0 µm. FISH images were analyzed using FISHQUANT[98]. Briefly, after background subtraction, the FISH spots in the cytoplasm were fit to a three-dimensional (3D) Gaussian to determine the coordinates of the mRNAs. The intensity and width of the 3D Gaussian were thresholded to exclude nonspecific signal. The average intensity of all the mRNAs was used to determine the intensity of each transcription site.

Quantification of peripheral distribution index

The peripheral distribution index (PDI) was quantified as described in[87]. Briefly, the Matlab-based software RDI (RNA dispersion index) calculator was used to calculate the peripheral distribution index for each cell by identifying cellular RNAs and describing their distribution in relation to the nucleus. Prior to analysis with the RDI calculator, the RNA channel was processed using a 3D Laplacian of Gaussian filter of radius=5 and standard deviation=1. The cell and nucleus channels were processed using the brightness/contrast function in ImageJ to enhance the contrast between the object and the background, as advised in[87].

Co-localization analysis

The RNA-RNA co-localization analysis reported in **Fig. 3S f-g** was performed using FISH-quant as described in[99]. Briefly, FISH-quant performs the co-localization analysis in each cell separately by treating the assignment as a Linear Assignment Problem (LAP). The two spot detection results (x, y, z positions) are considered as 3D point clouds. The Hungarian algorithm solving the LAP

finds the best possible global assignment between these two points-clouds such that for each point in the first channel, the closest point in the second channel is found. LAP has the important property that assignment is exclusive; one point from the first channel can be linked to at most one point from the other channel, and conversely. The linking is also globally optimal because the sum of the squared distance is minimized. This analysis is implemented using the Matlab functions hungarianlinker2 and munkres3.

For the co-localization of *CLB2* mRNA and protein foci, the FISH-quant data for the individual molecules were used as x, y, z coordinates and euclidean distances for all protein - mRNA molecule combinations were calculated in the mother and daughter cells. Protein and mRNA molecules closer than 250 nm were considered to be in a translation complex. Multiple protein molecules can be within 250 nm of a single mRNA molecule, and this would still be considered a single translation complex.

PDE solution for mRNA diffusion

We use a modified diffusion equation at steady state to model the mRNA movement in terms of diffusion of a concentration *c(x,y,z)* in 3 spatial dimensions, and include binding to ribosomes (uniformly spread) leading to the formation of complexes *b(x,y,z)*:

$$0 = D \cdot \nabla^2 c(x,y,z) - k_d \cdot c(x,y,z) + k_p - k_{\text{on}} \cdot c(x,y,z) + k_{\text{off}} \cdot b(x,y,z)$$

$$0 = k_{\text{on}} \cdot c(x,y,z) - k_{\text{off}} \cdot b(x,y,z) - k_d \cdot b(x,y,z)$$

With decay constant k_d = Ln(2)/$t_{0.5}$ = Ln(2)/240 s^{-1}, k_{on} = 0.25 (k_{off} + k_d) = 0.0035 and k_{off} = 1/90 = 0.011 chosen to reflect a half-life of 240 s, a 90 s mean lifetime of ribosome-bound complexes, and that approximately 20% of mRNAs appear bound at steady state. In the high-binding scenario k_{on} was increase by a factor of 125. For the numerical implementation, the production constant is represented by a small non-zero spread around the bud centre using a smooth step-function of which the volume integral is normalised to 1:

$$k_p = \frac{k_{max} \cdot e^{s \cdot m}}{e^{m \cdot r} + e^{s \cdot m}}$$

For the simulation results shown in Fig. 5S, the values chosen are s = 5 and m = 10, and the normalization results in k_{max} = 0.0019. Although the exact value of this constant affects the absolute concentration of mRNA it does not affect the ratio of mother to bud RNA. The PDE is solved in three Cartesian coordinates using the FEM implementation in Wolfram Mathematica (Wolfram Research, Inc., Mathematica, Version 12.3.1, Champaign, IL).

Ellipsoid fitting to mother and bud DIC images

Differential interference contrast (DIC) images were analysed in Mathematica to fit 3D ellipsoids to mother and bud models. X- and y-axes length were measured for the cells and the short axis was used as estimation of the z-axis. The z-axis origin value was aligned with the z-stack images by maximising the Fish-Quant mRNA and protein point inclusions.

Pattern search to predict ZIP-codes and synonymization

To identify potential ZIP-codes in the *CLB2* mRNA, we performed a targeted pattern search (Seiler et al., manuscript in preparation). In the first step, we leniently screened for two nested pairs of inverted repeats with a minimal length of four nucleotides that framed an asymmetric bulge region as found in the E3 ZIP-code in the *ASH1* mRNA[84]. We also checked for the presence of a CGA motif and a singular cytosine on the opposite strand with a defined distance of six nucleotides[100]. The search was performed on the complete *CLB2* mRNA with 1476 nt of CDS (YPR119W; genomic coordinates: chromosome XVI, 771653-773128, +, genome version S288C; *Saccharomyces* Genome Database, https://www.yeastgenome.org/locus/S000006323). We further added 366 nt 3' UTR and 346 nt 5' UTR as previously determined by[55]. In the second step, the minimum free energy (MFE) folds of all initial instances were analyzed using RNAfold with and without including a constraint on the nested pairs of inverted repeats[101,102]. Fold prediction was performed at 28°C with 80 nt RNA sequence fragments centered on each instance. Instances

were only kept if (i) at least one of inverted repeat pairs was present in the MFE structure without constraints, and (ii) the free energy (ΔG) of the constraint structure did not differ by more than 20% from the MFE structure without constraint. The latter accounts for energetic benefits from interaction with the She2-She3 proteins. The pattern search predicted a single ZIP-code at nucleotide positions +1111 to +1145 of the CDS (genomic coordinates: chromosome XVI, 772763-772797, +). **Fig. 4c** displays the predicted fold with constraint using RNAfold of ZIP-code instance plus ±5 nt flanking sequence. Visualization of the predicted structure in dot-bracket notation was generated using VARNA[103]. Repeating the pattern search described above on the synonymized ZIP-code mutant did not retrieve any hits. The complete sequences of the synonymized ZIP-code mutant are provided in the Resource Table.

Sample preparation for live yeast fluorescence imaging

Yeast cells were grown at 26°C in synthetic selective medium. Exponentially growing cells (OD_{600} 0.2-0.4) were plated on coated Delta-T dishes (Bioptech 04200417C). The dishes coating was done by incubating with Concanavalin A 1mg/ml (Cayman chemical company) for 10 minutes at room temperature. Excess liquid was aspirated and dishes were dried at room temperature. To activate Concanavalin A, dishes were incubated for 10 minutes at room temperature with a 50 mM $CaCl_2$ 50 mM $MnCl_2$ solution. Excess was removed and dishes dried at room temperature. Finally, dishes were washed once with ultrapure water (Invitrogen) and completely dried at room temperature. Cell attachment was performed by gravity for 20 minutes at room temperature, excess liquid removed and substitution with fresh media. Cells were diluted to OD_{600} 0.1 and grown until OD_{600} 0.3-0.4. before being plated on Concanavalin A coated dish.

Live cell fluorescence imaging and image analysis

The two-color simultaneous imaging of mRNAs and the appropriate cellular marker was performed on a modified version of the home-built microscope described in[67,68]. Briefly, the microscope was built around an IX71 stand (Olympus). For excitation, a 491 nm laser

(CalypsoTM, Cobolt) and a 561 nm laser (JiveTM, Cobolt) were combined and controlled by an acoustic-optic tunable filter (AOTF, AOTFnC-400.650-TN, AA Opto-electronic) before coupled into a single mode optical fiber (Qioptiq). The output of the fiber was collimated and delivered through the back port of the microscope and reflected into an Olympus 150x 1.45 N.A. Oil immersion objective lens with a dichroic mirror (zt405/488/561rpc, 2mm substrate, Chroma). The tube lens (180 mm focal length) was removed from the microscope and placed outside of the right port. A triple band notch emission filter (zet405/488/561m) was used to filter the scattered laser light. A dichroic mirror (T560LPXR, 3mm substrate, Chroma) was used to split the fluorescence onto two precisely aligned EMCCDs (Andor iXon3, Model DU897) mounted on alignment stages (x, y, z, θ- and φ- angle). Emission filters FF03-525/50-25 and FF01-607/70-25 (Semrock) were placed in front of green and red channel cameras, respectively. The two cameras were triggered for exposure with a TTL pulse generated on a DAQ board (Measurement Computing). The microscope was equipped with a piezo stage (ASI) for fast z-stack and a Delta-T incubation system (Bioptech) for live-cell imaging. The microscope (AOTF, DAQ, Stage and Cameras) was automated with the software Metamorph (Molecular Devices). For two-color live-cell imaging, yeast cells were streamed at 50 ms, Z plane was streamed, and z-stacks acquired every 0.5 µm. Single-molecule analysis was done on maximal projected images using Fiji. Maximally projected images were filtered using the Maxican Hat filter (Radius=2) in Fiji. Spots were identified and counted using the spot detection plugin integrated in TrackMate. LoG detector was used for the spot identification, object diameter= 3 and Quality threshold = 2500. Files were exported as csv files and plotted using GraphPad Prism.

Deconvolution algorithm

To reduce imaging artifacts arising from noise and optics of the microscope, we used the Huygens software v3.6, where a Classic Maximum Likelihood Estimation (CMLE) algorithm was applied as a restoration method to deconvolve the images used for protein-mRNA foci co-localization (**Fig.**

5). CMLE assumes the photon noise to be governed by Poisson statistics and optimizes the likelihood of an estimate of an object in the input 3D image while taking the point spread function into consideration. The CMLE deconvolution method was chosen since it is suited for images with low signal-to-noise ratio and to restore point-like objects. The result is a more accurate identification of the location of the object, which in our case is the fluorescently labeled mRNA and protein molecules. The restoration parameters used with the CMLE deconvolution algorithm was 99 iterations, a quality stop criterion of 0.01, and a signal-to-noise ratio of 15.

CLB2 mRNA bud localization quantification in living cells

For the analysis reported in **Fig. 2e**, the ImageJ plugin Labkit (https://imagej.net/Labkit) was manually used to segment cells and RNAs. Segmented cells were used as input for training the deep learning program Stardist in 2 dimensions. Stardist was used to automatically detect and segment cells and single mRNAs from live imaging movie frames (Cell Detection with Star-convex Polygons, https://arxiv.org/pdf/1806.03535.pdf). Cell and RNA segmentation was imported into R using the RImageJROI package. In R, the cell size, number of mRNAs in the bud and the distance of each bud localized mRNA to the periphery was calculated and plotted over time using the R packages Spatial Data and PBSmapping[104]. The Stardist segmentations were used to plot the RNAs and the cell's periphery onto the live imaging movie using the FFmpeg wrapper function for the FFmpeg multimedia framework (https://ffmpeg.org/).

Protein extraction and Western blot

Yeast strains were grown overnight at 26°C in yeast extract peptone dextrose (YEPD) medium with 2% glucose. In the morning, cells were diluted to OD_{600} 0.1 and allowed to grow until OD_{600} 0.5-1. Cell lysis was performed by adding 1 ml H_2O with 150 µl of Yex-lysis buffer (1.85 M NaOH, 7.5% 2-mercaptoethanol) to the pellet of 3-5 ODs of cells (~$3x10^7$) and kept 10 minutes on ice. Proteins were precipitated by the addition of 150 µl of TCA 50% for 10 minutes on ice. Cells were pelleted and resuspended in 100 µl of 1X sample buffer (1 M Tris-HCl pH 6.8, 8 M Urea, 20%

SDS, 0.5 M EDTA, 1% 2-mercaptoethanol, 0.05% bromophenol blue). Total protein extracts were fractioned on SDS-PAGE and examined by Western blot with mouse anti-Myc (Sigma), mouse anti-Pgk1 (Thermofisher). For quantitative Western blot analyses, fluorescent secondary α-Mouse (IRDye 800CW) and α-Rabbit (IRDye 680RD) antibodies were used. The signals were revealed using the LYCOR® scanner and quantified using LITE® Software.

Growth curves setup and analysis

Cells were grown overnight at 30°C in SC-complete or Drop-out medium with 2% glucose. Cells in mid-log phase were spun down, the supernatant was removed and cells were resuspended at a final OD_{600} of about 0.1 in test medium containing different carbon sources, as indicated in the figure legend. In 48-well plates with flat bottom, 400 µl were plated per well. At least 3 well replicates were done per experiment. Cells were grown for the indicated time, at 30°C. OD_{600} measurements were taken every 5 minutes, with 700 rpm shacking between time-points using a CLARIOstar® plate reader (BMG Labtech). Growth curves analysis was performed using an adaptation of the R package Growthcurver[105] and plotted using the R package ggplot2[106], tydiverse[107], RColorBrewer[108], dplyr[109]. Growthcurver fits a basic form of the logistic equation to experimental growth curve data. The logistic equation gives the number of cells N_t at time t.

$$N_t = \frac{K}{1 + \left(\frac{K - N_0}{N_0}\right) e^{-rt}}$$

The population size at the beginning of the growth curve is given by N_0. The maximum possible population size in a particular environment, or the carrying capacity, is given by K. The intrinsic growth rate of the population, r, is the growth rate that would occur if there were no restrictions imposed on total population size. Growthcurver finds the best values of K, r, and N_0 for the growth curve data using the implementation of the non-linear least-squares Levenberg-Marquardt algorithm. The carrying capacity and growth rate values (K and r) are used to compare the growth dynamics of strains.

Flow cytometry sample preparation and analysis

Cells were grown overnight at 30°C in SC-complete medium with 2% glucose. Cells were grown to mid-log phase (OD_{600} 0.3-0.4) with constant shacking (220 pm) at 30°C. Next, they were spun down, the supernatant was removed and cells were resuspended at a final OD_{600} of about 0.1 in test medium containing different carbon sources, as indicated in the figure legend. At the indicated time-points, 1 mL of culture was transferred to a 1.5 mL Eppendorf tube and centrifuged for 3 minutes at 3000 rpm. The supernatant was removed and cells were resuspended in 70% ethanol and incubated overnight at 4°C. Cells were washed once with 1xPBS pH 7.4 and resuspended in 500 µl of 1xPBS with 1 µl of RNAse A 1 mg/mL and incubated at 37°C for at least 3 hours. Cells were then washed with 1 mL of 1xPBS and resuspended in 500 µl of 1xPBS. 100 µl of cells were then incubated with 3 µl of a 5 µM solution of Sytox Orange and incubated in a water bath at 37°C for 3 hours covered from the light. Cells were then washed 3 times with 1xPBS and resuspended in 500 µl of 1xPBS. The cells were then analyzed with the Backman Culter Flow cytometer CytoFLEX S System (B2-R0-V2-Y2). A 561 nm laser was used to excite the fluorescent dye and a band pass filter was used to filter the emitted fluorescence. 50'000 cells were collected per sample. Analysis and plotting was performed using R Studio and the following R packages: ggplot2[106]; tydiverse[107], RColorBrewer[108], dplyr[109], mixtools[110].

Quantifications and statistical analysis

FISH-quant was used to quantify single mRNA molecules and protein foci in fixed samples. Fiji was used to quantify single mRNA molecules in living cells. GraphPad Prism was used to calculate the mean and the standard deviation (SD) of all the data and perform statistical analysis. Flow cytometry data, growth curves analysis was performed in R Studio, as detailed in previous paragraphs. For each experiment, the number of biological replicates, the number of cells analyzed (n), statistical analysis applied and significance ($P<0.05$ for significant differences) is indicated in the figure legend or in the main text.

Figure Legends

Figure 1. CLB2 mRNAs localize to the bud in a cell-cycle dependent manner.

(a) Schematic of *CLB2* mRNA expression during the cell cycle. Green dots represent *CLB2* mRNAs. The Whi5 protein (cyan) accumulates in the nucleus during early G1 phase[72,111,112]. Tubulin (magenta) is a major component of microtubules and the mitotic spindle. Bud emergence starts during S phase and ends with the formation of the daughter cell. During anaphase, the microtubules stretch between the mother and the daughter cell. **(b)** Top panels: MERGE Maximal projections of IF anti-HA (Whi5) (cyan) and DAPI (blue) merged to a single differential interference contrast (DIC) section (grey). Bottom panels: MERGE Maximal projections of *CLB2* mRNA smFISH (green), anti-tubulin IF (magenta) and DAPI (blue) merged to a single DIC section (grey). The corresponding cell cycle phase is indicated on the panels. Scale bars 3 μm. **(c)** smFISH quantifications of *CLB2* mRNA expression during the different cell cycle phases determined using the markers shown in (b). Dots correspond to individual cells (2083 cells, from two replicates). The black bar indicates the average (G1 early= 1.2±1.9; G1 late= 1.2±1.9; S= 3.8±3.0; G2= 10.3±5.7; M= 8.0±6.5 mRNAs/cell mean ± standard deviation [SD]). **(d)** Relative bud vs mother distribution of the *CLB2* mRNA in WT budded cells based on the smFISH-IF data shown in (b) (mean ± SD).

Supplementary Figure 1. CLB2 mRNAs are synthesized and localized in the bud in a cell-cycle dependent manner.

(a) Quantification of *CLB2* mRNA smFISH shown in Figure 1b reported as relative frequency distribution of mature mRNAs per cell. Data from two replicates (n=2083). **(b)** Quantification of *CLB2* nascent RNAs at transcriptions sites (TS) from smFISH shown in Figure 1b reported as relative frequency distribution of nascent RNAs per TS. Data from two replicates (n=2083). **(c)** MDN1 smFISH maximal projection (green), and DAPI merged to a single DIC section (grey). Scale bar 5 μm **(d)** Relative bud vs mother distribution of *MDN1* mRNA in budded cells based on

the smFISH data shown in (b). Data from two replicates (n=2011; mean ± SD). **(e)** smFISH in the *S. cerevisiae* background W303. MERGE Maximal projections of *CLB2* mRNA smFISH (green) and DAPI (blue) merged to a single DIC section (grey). Scale bar 3 µm.

Figure 2. CLB2 mRNA imaging in living cells reveals a rapid mRNA synthesis and degradation and localization to the bud.

(a) Schematic of *CLB2* localization during the cell cycle. The *CLB2* mRNA (green) is expressed from late S-phase and localizes to the emerging bud. Bud emergence as well as the separation of the bud from the mother can be identified by endogenously tagging the bud neck protein Cdc10 with tdTomato (magenta). The *CLB2* mRNA is rapidly degraded during mitosis. **(b)** *CLB2* endogenously tagged with 24xMBSV6 to enable visualization of the mRNA (black) in live cells. The bud neck protein Cdc10 is tagged with tdTomato (magenta). Cell A is the mother of cell B. Time point from start of acquisition is indicated in the upper left corner of each time frame. Scale bar 3 µm. **(c)** Percentage of *CLB2* mRNAs localized in the bud over time from bud appearance. **(d)** Number of *CLB2* mRNAs per cell over time in cell A and cell B. **(e)** Snap shots from live cell imaging of *CLB2* mRNA endogenously tagged with 24xMBSV6 (green). Approximate cell outline identified from fluorescent background (orange). A single Z plane was acquired every 100 ms. Scale bars 3 µm **(f)** Average cell area monitored over time in live cells (n=3). A single Z plane was acquired every 100 ms. Lower right insert shows cell size of a single cell acquired every 2 min. Red line in insert indicates when the 100 ms images were acquired. Pink, purple and green lines represent time points at which the snapshots in (e) were taken. **(g)** Average number of bud localized mRNAs per cell over time as monitored from 3 single cells. Pink, purple and green lines represent the time points at which the snapshots in (e) were taken.

Supplementary Figure 2. CLB2 mRNAs endogenously tagged with the MBSV6 reporter recapitulate the expression of the endogenous CLB2 mRNA.

(a) Schematic of *CLB2* locus endogenously tagged with 24xMBSV6 inserted in the 3' UTR after the STOP codon. Dotted lines represent smFISH probe positions targeting the CDS (green) or MBS sequences (magenta). **(b)** Two-color smFISH for cells expressing tagged *CLB2* mRNAs. Top panels (MBSV6), cells expressing the control vector (YcpLac111). Bottom panels (MBSV6+MCP) cells expressing MCP (YcpLac111 CYC1p-MCP-NLS-2xyeGFP). DIC/MERGE shows the overlap of the DAPI signal in the nucleus (blue), smFISH for the *CLB2* CDS (green) and the MBS (magenta) with the differential interference contrast (DIC) image. Scale bars 3 μm. **(c)** Quantification of smFISH represented in 4b as well as untagged WT cells, with CDS probes (green plots) or MBS probes (magenta) reported as distribution of mature mRNAs per cell. Mean of three biological replicates, (*CLB2* MBSV6: CLB2 probes n= 862, mean ± SD 4.9 ± 5.8 mRNA/cell; MBSV6 probes n=738, mean ± SD 5.1 ± 5.6 mRNA/cell; *CLB2* MBSV6+MCP: *CLB2* probes n = 752, mean ± SD 4.7± 5.3 mRNA/cell, MBSV6 probes n=974, mean ± SD 4.7±4.9 mRNA/cell; WT cells: *CLB2* probes n = 791). **(d-e)** Correlation between the number of single CDS and MBSV6 molecules per cell in presence or absence of MCP. Pearson *r* values calculated by combining two independent experiments (n=1908 and 2284, respectively). **(f)** Average number of *CLB2* mRNA per cell tagged with 24xMBSV6 monitored over time. Grey represents SD from average mRNA per cell (purple).

Figure 3. The She2-3 complex and an RNA ZIP code in CLB2 mRNA CDS are required for bud localization.

(a) smFISH-IF in WT (top row), *Δshe2* (middle row), and *Δshe3* (bottom row) cells. MERGE Maximal projections of *CLB2* mRNA smFISH (green), anti-tubulin IF (magenta) and DAPI (blue) merged to a single DIC section (grey). The corresponding cell cycle phase is indicated on top of the panel. Scale bars 3 μm. **(b)** Schematic of *CLB2* mRNA coding sequence. The blue box

represents the ZIP-code at nucleotides 1111-1145 (relative to START codon). **(c)** Predicted secondary structure of ZIP-code (blue box) with flanking sequence (nt 1089- 1168). The free energy (ΔG) of the mRNA folding is indicated. **(d)** Synonymized ZIP code (*ZIP-mut*). Top sequence is *CLB2* WT. Bottom sequence is the synonymized sequence. Mutated nucleotides are indicated in red. Below is the corresponding Clb2 protein amino acid sequence, which is identical for both the WT and synonymized strains. Rare amino acid codons were avoided to maintain the same codon optimization index = 0.74. **(e)** smFISH in WT and ZIP-code mutant strain. Maximal projections of smFISH with *CLB2* probes (green) and DAPI (blue) and fluorescence images overlapped to a single DIC section (MERGE). Scale bars 3 μm. **(f)** Relative bud vs mother distribution of the *CLB2* mRNA in WT and ZIP-code mutant strain based on smFISH-IF data shown in (e). **(g)** Schematic representation of mRNA peripheral distribution index (PDI). Black dots represent mRNA. Blue is the nucleus. A PDI close to 0 indicates that the RNA of interest is localized near the nucleus. A PDI of 1 indicates that the RNA is diffusely dispersed throughout the cell. As the PDI value grows > 1, the polarization of the mRNA increases. **(h)** PDI in WT cells for *ASH1*, *CLB2* and *MDN1* mRNAs and in *Δshe2*, *Δshe3* and ZIP-code mutant strains for the *CLB2* mRNA. Index values are calculated from smFISH-IF experiments shown in (e) and **Fig. 3Sa**.

Supplementary Figure 3. CLB2 is not co-localized to the bud together with the ASH1 mRNA.

(a) WT, *Δshe2* and *Δshe3* cells: Left panels, MERGE Maximal projections of *CLB2* mRNA smFISH (green), anti-tubulin IF (magenta) and DAPI (blue) merged to a single DIC section (grey). Right panels, MERGE Maximal projections of IF anti-HA (Whi5) (cyan) and DAPI (blue) merged to a single DIC section (grey). Scale bars 5 μm. **(b)** Relative bud vs mother distribution of the *CLB2* mRNA in *Δshe2* budded cells based on the smFISH-IF data shown in **Fig.3a** and **Fig.3Sa**. **(c)** Relative bud vs mother distribution of the *CLB2* mRNA in *Δshe3* budded cells based on the smFISH-IF data shown in **Fig. 3a** and in **Fig. 3Sa**. **(d)** Schematic of *CLB2* and *ASH1* mRNAs

expression during the cell cycle. Green dots represent *CLB2* mRNAs. Magenta dots represent *ASH1* mRNAs. Tubulin (grey) co-localizes with the spindle pole body which is duplicated during S phase. The bud emergence starts during S phase and ends with the formation of the daughter cell. During anaphase, the microtubules stretch between the mother and the daughter cell **(e)** MERGE Maximal projections of *CLB2* mRNA smFISH (green), *ASH1* mRNA smFISH (magenta), anti-tubulin IF (white) and DAPI (blue) merged to a single DIC section (grey). The corresponding cell cycle phase is indicated on top of the panel. Scale bars 3 µm. **(f)** Percentage of co-localized *ASH1* and *CLB2* mRNAs (<250 nm) over total amount of *ASH1* and *CLB2* mRNA, from S phase to mitosis (in budded cells co-expressing both mRNAs) (mean ± SD). We found 10.3% of *ASH1* mRNA and 7.7% of *CLB2* mRNAs to co-localize, suggesting that *CLB2* and *ASH1* mRNAs are not co-transported. **(g)** Example of 2-color smFISH colocalization analysis performed using FISH-quant V3, FQ_DualColor_cololocalization function[99]. Colocalization between the two channels was calculated as a linear assignment problem (LAP) solved with the Hungarian algorithm using the Matlab function "hungarianlinker" and "munkres". We defined the maximum 3D allowed distance between two spots to be considered co-localized to 250 nm (~3 pixels). Left, MERGE maximal projection of filtered smFISH channels, *CLB2* (green) and *ASH1* (magenta). Right, color-coded localization of mRNAs by smFISH: Blue, co-localized (co-loc); Red, not-co-localized mRNAs; Yellow, not-co-localized in the other channel. **(h)** Previous structural work demonstrated that the She2-She3 complex comprises two She2 and She3 dimers, which can bind two mRNA targets simultaneously[84]. Comparison of RNA spots intensities distributions by smFISH in WT or ∆she2 and ∆she3 mutants was used to examine whether *CLB2* mRNAs are transported to the bud two-by-two by. Two mRNAs in close proximity (<250 nm) would be detected as a single bright spot due to the microscope diffraction limit. A drop in *CLB2* mRNA spot intensities in the She mutants would indicate co-transported mRNAs. Relative frequency distribution of *CLB2* mRNA spot intensities in WT (n= 3004), *Δ*she2 (n= 2619) and *Δ*she3 (n= 2731) mutant strains (median WT = 45.7, lower 95% CI=45.0, upper 95% CI=46.8; *Δ*she2=40.4, lower 95% CI=39.1, upper 95%

CI=41.2; *Δshe3*=42.65, lower 95% CI=41.8, upper 95% CI=43.3). Results are shown for a representative experiment where the three strains were collected, processed and imaged side by side. A 3D Laplacian of Gaussian filter was applied to all the images using FISH-quant. The mean and SD of spot intensities are expressed as arbitrary units (a.u.).

Figure 4. CLB2 mRNA mislocalization affects Clb2 protein expression but not mRNA levels, protein stability or localization.

(a) smFISH quantifications of *CLB2* mRNA expression in WT and localization mutants. Dots correspond to individual cells (~1000 cells per replicate, from at least 2 replicates). The black bar indicates the average (mRNAs/cell mean ± SD). **(b)** Quantification of nascent *CLB2* RNAs at transcription sites (TS) from smFISH. Dots correspond to individual cells (~1000 cells per replicate, from at least 2 replicates). Visualization as in (a). **(c)** Western blot analysis using anti-myc antibody against Clb2 protein endogenously tagged with 5 myc tags in WT, *Δ*she2, *Δ*she3 and ZIP-code mutant cells. First lane is the control untagged strain. Endogenous Pgk1 was used as loading control **(d)** Quantification of western blot in (c). Myc signal normalized to Pgk1 loading control. Protein levels relative to WT indicated in lower bar. Mean ± SD from 3-7 replicates. **(e)** Clb2 protein stability assay in WT, *Δ*she2 and *Δ*she3 cells. Western blot was performed using an anti-myc antibody to target Clb2 protein tagged with 5 myc tags in cells treated with 100 µg/ml cycloheximide for 0, 5, 10, 20, 30 45, or 60 minutes. Pgk1 was used as loading control. **(f)** Clb2 protein stability assay in WT and ZIP-code mutant. Western blot was performed in the same way as in (c). **(g)** Clb2 fused to yeGFP in WT, *Δ*she2, *Δ*she3 and ZIP code mutant cells. Maximal projections of Clb2-GFP (green) overlapped to a single DIC section. Scale bars 2 µm.

Supplementary Figure 4. CLB2 mRNA mislocalization is not affecting protein stability but it correlates with delayed Clb2 protein accumulation.

(a) Growth curves of strains with Myc-tagged Clb2 protein performed in SC-complete 2% glucose at 26°C. Growth rates (r), calculated by fitting the data to a logistic curve, are provided in the

associate table. **(b)** Example of western blot of Clb2 protein stability assay in WT, *Δ*she2 and *Δ*she3 cells. Western blot was performed using an anti-myc antibody to target Myc-tagged Clb2 protein tagged in cells treated with 100 µg/ml cycloheximide for 0, 5, 10, 20, 30 45, or 60 minutes. Pgk1 was used as loading control. Quantifications are reported in **Fig. 4e**. **(c)** Example of western blot of Clb2 protein stability assay in WT and ZIP-code mutant cells. Western blot was performed using an anti-myc antibody to target Clb2 protein tagged with 5 myc tags in cells treated with 100 µg/ml cycloheximide for 0, 5, 10, 20, 30 45, or 60 minutes. Pgk1 was used as loading control. Quantifications are reported in **Fig. 4f**. **(d)** Quantification of Clb2-GFP expression measured in living WT and *Δ*she2 cells. Cells were grown in SC-complete 2% glucose at 26°C. Images were collected every 5 minutes, 13 Z planes were acquired every 0.5 µm, with an exposure time of 50 ms. Maximally projected images were used for cell segmentation and quantification of GFP integrated intensity (expressed as arbitrary units a.u.). **(e)** Correlation of Clb2-GFP expression and bud volume measured in living WT and *Δ*she2 cells.

Figure 5. CLB2 mRNA and protein colocalization indicates preferential translation in the bud.

(a) smFISH-IF in WT cells. Top panels: MERGE Maximal projections of IF anti-tubulin (cyan) and DAPI (blue) merged to a single DIC section (grey). Second panel row from the top: MERGE Maximal projections of IF anti-myc-Clb2 protein (magenta), *CLB2* mRNA smFISH (green) and DAPI (blue) merged to a single DIC section (grey). The third and fourth panels from the top are the *CLB2* mRNA smFISH and Clb2 protein IF, respectively. Scale bars 3 µm. **(b)** Quantification of protein clusters in WT bud (B) and mother (M) cells from IF experiments shown in (a). Cell cycle classification was performed using tubulin and DAPI as markers. **(c)** Quantification of mRNA in WT bud (B) and mother (M) cells from smFISH experiments shown in (a). Cell cycle classification was performed as in (b). **(d)** smFISH-IF in Δshe2 cells. Maximal projections of IF anti-myc-Clb2 protein (magenta), *CLB2* mRNA smFISH (green) and DAPI (blue) merged to a single DIC section (grey). Panels description as in (a). Scale bars 2 µm. **(e)** Quantification of *CLB2*

mRNA-protein clusters found in close proximity (<250 nm) by smFISH-IF experiments performed in bud (B) and mother (M) cells of WT and Δshe2 cells shown in panels (a) and (d). **(f)** Quantification of bud-localized mRNAs co-localizing with a protein cluster (<250 nm) in WT and Δshe2 cells shown in panels (a) and (d).

Supplementary Figure 5. Translation inhibition with cycloheximide causes CLB2 mRNA stabilization and correlates with reduced mRNA localization in the bud

(a) Schematic of the *CLB2* endogenous gene tagging to simultaneously visualize single mRNA by smFISH and Clb2 proteins by IF in fixed cells. 25 myc tags are inserted into the 5' end of the *CLB2* CDS. smFISH is performed against the *CLB2* CDS (top panel). As the mRNA is being translated the myc tags will be first to emerge from the ribosome and will be detectable with IF (bottom panel). By performing smFISH against the *CLB2* mRNA and IF against the 25xmyc-tagged Clb2 protein, translation can be detected by the co-localization of the two signals. **(b)** Western blot analysis of CLB2 Myc tagged strains. Top row is the myc signal. Bottom row is the Pgk1 loading control. First lane is untagged cells. Second and third lanes are the Clb2 protein tagged with 5 and 25 myc tags, respectively. **(c)** smFISH-IF in WT cells treated with 100 µg/mL of translation elongation inhibitor cycloheximide (CHX) for 20 min. Top panels: MERGE Maximal projections of IF anti-tubulin (cyan) and DAPI (blue) merged to a single DIC section (grey). Second panel row from the top: MERGE Maximal projections of IF anti-myc-Clb2 protein (magenta), *CLB2* mRNA smFISH (green) and DAPI (blue) merged to a single DIC section (grey). The third and fourth panels from the top are the *CLB2* mRNA smFISH and Clb2 protein IF, respectively. Scale bars 3 µm. **(d)** smFISH quantifications of *CLB2* mRNA expression of cells exposed to CHX shown in (b). Dots correspond to individual cells (46 cells, from two replicates). **(e)** smFISH quantifications of *CLB2* mRNA expression in bud (B) and mother (M) cells exposed to CHX shown in (b). Dots correspond to individual cells (46 cells, from two replicates). **(f)** Quantification of *CLB2* mRNA-protein clusters found in close proximity (<250 nm) by smFISH-IF experiments performed

in buds (B) and mothers (M) of WT cell exposed to CHX shown in (b). **(f)** PDE simulation results of ribosome binding scenarios using concentration distribution at steady state for normal binding at diffusion D = 400'000 nm^2/s; **(g)** at D = 100'000 nm^2/s. **(h)** Concentration distribution at steady state for high binding and D = 100'000 nm^2/s. Units: length nm, time s, concentration $1/nm^3$. Note that the colors have been log-scaled.

Figure 6. Known translation inhibitors are not involved in regulating Clb2 protein expression

(a) Western blot analysis using anti-myc antibody against Clb2 protein tagged with 25 myc tags in WT, *Δssd1, Δkhd1* and *Δpuf6* cells. Pgk1 was used as loading control. First lane is untagged cells. **(b)** Quantification of (a). Mutant strain signal is normalized to WT signal. Each color corresponds to one replicate experiment. Black bar indicates mean ± SD (WT= 100; Δssd1= 88.3±15.6; Δkhd1= 98.8±13.5; Δpuf6= 83.9±10.4). **(c)** Merge maximal projections of *CLB2* smFISH (green), DIC (gray), and DAPI (blue) in WT, *Δssd1, Δkhd1* and *Δpuf6* cells. Scale bars 5 µm. **(d)** Quantification of *CLB2* smFISH in WT, *Δssd1, Δkhd1* and *Δpuf6* cells. Each dot corresponds to a single cell (500-1500 cells from two to four replicates). Each color corresponds to one replicate. Black bar indicates the average (WT= 4.3±0.5; Δssd1= 4.8±0.8; Δkhd1= 4.2±0.7; Δpuf6= 6.9±1.2 mRNAs/cell mean ± SD). **(e)** smFISH quantification of nascent *CLB2* RNA expression per transcription site in WT, Δssd1, Δkhd1 and Δpuf6 cells. Dots correspond to individual cells (500-1500 cells from two to four replicates). Each color corresponds to one replicate. Black bar indicates the average (WT= 2.4±1.1; Δssd1= 2.6±1.0; Δkhd1= 2.1±0.7; Δpuf6= 2.5±1.1 mRNAs/transcription site ± SD).

Supplementary Figure 6. Known translation inhibitors are not involved in regulating CLB2 local translation, but Puf6 regulates CLB2 transcription.

(a) Relative frequency distribution of mature *CLB2* mRNAs per cell. **(b)** Merge maximal projection of *CLB2* smFISH (green), DIC (gray), and DAPI (blue) in a *Δpuf6* cell. Yellow arrows indicate

transcription sites. Scale bar 2 µm. **(c)** Quantification of transcription sites in transcriptionally active WT and *Δpuf6* cells (n = 1340 and 1583 cells, respectively) based on *CLB2* mRNA smFISH.

Figure 7. The CLB2 mRNA ZIP code mutants show clone-dependent growth defect and cell cycle defect.

(a) Top, single *CLB2* ZIP-code mutant clones grown on SC-complete 2% glucose at 30°C for 3 days. Bottom, *CLB2 ZIP*-code mutant clones from top plate were grown on SC-complete 0.1% glucose at 30°C for 3 days. **(b)** Tenfold serial dilutions of the indicated strains were spotted onto SC-complete plates at the indicated carbon sources and temperatures. **(c)** Growth curves of *CLB2* ZIP-code mutant clones (*ZIP cl1*, *cl2* and *cl3*) performed at 30°C in SC-complete at the indicated carbon sources. Optical density measurements (OD_{600}) were collected every 5 min. Triplicate experiments are shown for each strain. **(d)** Cell cycle analysis by DNA content estimation with flow cytometry in the ZIP-code mutants grown at the indicated conditions. DNA was stained with Sytox Orange. Mixed Gaussian fitting (black lines) was used to estimate the indicated G1 and G2/M components. Percentages are reported for one representative experiment.

Supplementary Figure 7. CLB2 ZIP code mutant cells shows a growth defect and clonal variability under nutrient limited conditions

(a) Growth curves of *SHE* deleted strains (Δ*she2*, Δ*she3*) performed at 30°C in SC-complete at the indicated carbon sources. Optical density measurements (OD_{600}) were collected every 5 min. Triplicate experiments are shown for each strain. **(b)** Left, Bright-field images of WT or *CLB2* ZIP-*cl1* mutant grown in SC-complete 2% glucose at 30°C. Right, quantification of WT and *CLB2* ZIP-code cl1 mutant cell areas. **(c)** Growth curves of Diploid strains generated by crossing WT cells (mating type *alpha*) with either (mating type *a*) WT or the *CLB2* ZIP-code cl1 mutant, performed at 30°C in SC-complete at the indicated carbon sources. Triplicate experiments are reported for each strain.

References

1. Lecuyer, E. *et al.* Global analysis of mRNA localization reveals a prominent role in organizing cellular architecture and function. *Cell* **131**, 174–87 (2007).
2. Nevo-Dinur, K., Nussbaum-Shochat, A., Ben-Yehuda, S. & Amster-Choder, O. Translation-Independent Localization of mRNA in E. coli. *Science* **331**, 1081–1084 (2011).
3. Martin, K. C. & Ephrussi, A. mRNA localization: gene expression in the spatial dimension. *Cell* **136**, 719–30 (2009).
4. Das, S., Vera, M., Gandin, V., Singer, R. H. & Tutucci, E. Intracellular mRNA transport and localized translation. *Nature Reviews Molecular Cell Biology* 1–22 (2021) doi:10.1038/s41580-021-00356-8.
5. Kejiou, N. S. & Palazzo, A. F. mRNA localization as a rheostat to regulate subcellular gene expression. *Wiley Interdiscip Rev RNA* **8**, (2017).
6. Becalska, A. N. & Gavis, E. R. Lighting up mRNA localization in Drosophila oogenesis. *Development (Cambridge, England)* **136**, 2493–503 (2009).
7. Cui, X. A. & Palazzo, A. F. Localization of mRNAs to the endoplasmic reticulum. *WIREs RNA* **5**, 481–492 (2014).
8. Buxbaum, A. R., Haimovich, G. & Singer, R. H. In the right place at the right time: visualizing and understanding mRNA localization. *Nature reviews. Molecular cell biology* **16**, 95–109 (2015).
9. Singer-Krüger, B. & Jansen, R.-P. Here, there, everywhere. mRNA localization in budding yeast. *RNA Biol* **11**, 1031–1039 (2014).
10. Shen, Z., Paquin, N., Forget, A. & Chartrand, P. Nuclear shuttling of She2p couples ASH1 mRNA localization to its translational repression by recruiting Loc1p and Puf6p. *Mol Biol Cell* **20**, 2265–75 (2009).
11. Long, R. M. *et al.* Mating type switching in yeast controlled by asymmetric localization of ASH1 mRNA. *Science* **277**, 383–7 (1997).

12. Takizawa, P. A. & Vale, R. D. The myosin motor, Myo4p, binds Ash1 mRNA via the adapter protein, She3p. *Proc Natl Acad Sci U S A* **97**, 5273–8 (2000).

13. Long, R. M. *et al.* Characterization of transport and localization of ASH1 mRNA in yeast. *Mol Biol Cell* **8**, 2060–2060 (1997).

14. Bertrand, E. *et al.* Localization of ASH1 mRNA particles in living yeast. *Mol Cell* **2**, 437–45 (1998).

15. Niessing, D., Huttelmaier, S., Zenklusen, D., Singer, R. H. & Burley, S. K. She2p is a novel RNA binding protein with a basic helical hairpin motif. *Cell* **119**, 491–502 (2004).

16. Long, R. M., Gu, W., Lorimer, E., Singer, R. H. & Chartrand, P. She2p is a novel RNA-binding protein that recruits the Myo4p-She3p complex to ASH1 mRNA. *Embo J* **19**, 6592–601 (2000).

17. Böhl, F., Kruse, C., Frank, A., Ferring, D. & Jansen, R.-P. She2p, a novel RNA-binding protein tethers ASH1 mRNA to the Myo4p myosin motor via She3p. *EMBO J* **19**, 5514–5524 (2000).

18. Deng, Y., Singer, R. H. & Gu, W. Translation of ASH1 mRNA is repressed by Puf6p-Fun12p/eIF5B interaction and released by CK2 phosphorylation. *Genes & development* **22**, 1037–50 (2008).

19. Gu, W., Deng, Y., Zenklusen, D. & Singer, R. H. A new yeast PUF family protein, Puf6p, represses ASH1 mRNA translation and is required for its localization. *Genes & development* **18**, 1452–65 (2004).

20. Irie, K. *et al.* The Khd1 protein, which has three KH RNA-binding motifs, is required for proper localization of ASH1 mRNA in yeast. *The EMBO journal* **21**, 1158–67 (2002).

21. Paquin, N. *et al.* Local activation of yeast ASH1 mRNA translation through phosphorylation of Khd1p by the casein kinase Yck1p. *Mol Cell* **26**, 795–809 (2007).

22. Hasegawa, Y., Irie, K. & Gerber, A. P. Distinct roles for Khd1p in the localization and expression of bud-localized mRNAs in yeast. *RNA* **14**, 2333–2347 (2008).

23. Shahbabian, K., Jeronimo, C., Forget, A., Robert, F. & Chartrand, P. Co-transcriptional recruitment of Puf6 by She2 couples translational repression to mRNA localization. *Nucleic Acids Res* **42**, 8692–8704 (2014).

24. Heym, R. G. & Niessing, D. Principles of mRNA transport in yeast. *Cell Mol Life Sci* **69**, 1843–53 (2012).

25. Niessing, D., Jansen, R.-P., Pohlmann, T. & Feldbrügge, M. mRNA transport in fungal top models. *Wiley Interdiscip Rev RNA* **9**, (2018).

26. Wanless, A. G., Lin, Y. & Weiss, E. L. Cell Morphogenesis Proteins Are Translationally Controlled through UTRs by the Ndr/LATS Target Ssd1. *PLOS ONE* **9**, e85212 (2014).

27. Jansen, J. M., Wanless, A. G., Seidel, C. W. & Weiss, E. L. Cbk1 Regulation of the RNA-Binding Protein Ssd1 Integrates Cell Fate with Translational Control. *Current Biology* **19**, 2114–2120 (2009).

28. Bayne, R. A. *et al.* Yeast Ssd1 is a non-enzymatic member of the RNase II family with an alternative RNA recognition interface. *bioRxiv* 2020.10.22.350314 (2020) doi:10.1101/2020.10.22.350314.

29. Ballou, E. R., Cook, A. G. & Wallace, E. W. J. Repeated evolution of inactive pseudonucleases in a fungal branch of the Dis3/RNase II family of nucleases. *bioRxiv* 2020.07.30.229070 (2020) doi:10.1101/2020.07.30.229070.

30. Shepard, K. A. *et al.* Widespread cytoplasmic mRNA transport in yeast: Identification of 22 bud-localized transcripts using DNA microarray analysis. *PNAS* **100**, 11429–11434 (2003).

31. Surana, U. *et al.* Destruction of the CDC28/CLB mitotic kinase is not required for the metaphase to anaphase transition in budding yeast. *The EMBO journal* **12**, 1969–78 (1993).

32. Fitch, I. *et al.* Characterization of four B-type cyclin genes of the budding yeast Saccharomyces cerevisiae. *Molecular biology of the cell* **3**, 805–18 (1992).

33. Amon, A., Irniger, S. & Nasmyth, K. Closing the cell cycle circle in yeast: G2 cyclin proteolysis initiated at mitosis persists until the activation of G1 cyclins in the next cycle. *Cell* **77**, 1037–50 (1994).

34. Örd, M. & Loog, M. How the cell cycle clock ticks. *MBoC* **30**, 169–172 (2019).

35. Surana, U. *et al.* The role of CDC28 and cyclins during mitosis in the budding yeast S. cerevisiae. *Cell* **65**, 145–161 (1991).

36. Amon, A., Tyers, M., Futcher, B. & Nasmyth, K. Mechanisms that help the yeast cell cycle clock tick: G2 cyclins transcriptionally activate G2 cyclins and repress G1 cyclins. *Cell* **74**, 993–1007 (1993).

37. Bloom, J. & Cross, F. R. Multiple levels of cyclin specificity in cell-cycle control. *Nature reviews. Molecular cell biology* **8**, 149–60 (2007).

38. Hood, J. K., Hwang, W. W. & Silver, P. A. The Saccharomyces cerevisiae cyclin Clb2p is targeted to multiple subcellular locations by cis- and trans-acting determinants. *Journal of Cell Science* **114**, 589–597 (2001).

39. Bailly, E., Cabantous, S., Sondaz, D., Bernadac, A. & Simon, M.-N. Differential cellular localization among mitotic cyclins from Saccharomyces cerevisiae: a new role for the axial budding protein Bud3 in targeting Clb2 to the mother-bud neck. *Journal of Cell Science* **116**, 4119–4130 (2003).

40. Hahn, S., Maurer, P., Caesar, S. & Schlenstedt, G. Classical NLS Proteins from Saccharomyces cerevisiae. *Journal of Molecular Biology* **379**, 678–694 (2008).

41. Eluère, R. *et al.* Compartmentalization of the functions and regulation of the mitotic cyclin Clb2 in S. cerevisiae. *J Cell Sci* **120**, 702–711 (2007).

42. Coudreuse, D. & Nurse, P. Driving the cell cycle with a minimal CDK control network. *Nature* **468**, 1074–1079 (2010).

43. Stern, B. & Nurse, P. A quantitative model for the cdc2 control of S phase and mitosis in fission yeast. *Trends in Genetics* **12**, 345–350 (1996).

44. Novak, B., Tyson, J. J., Gyorffy, B. & Csikasz-Nagy, A. Irreversible cell-cycle transitions are due to systems-level feedback. *Nat Cell Biol* **9**, 724–728 (2007).

45. Harvey, S. L. *et al.* A phosphatase threshold sets the level of Cdk1 activity in early mitosis in budding yeast. *MBoC* **22**, 3595–3608 (2011).

46. Kõivomägi, M. *et al.* Dynamics of Cdk1 Substrate Specificity during the Cell Cycle. *Mol Cell* **42**, 610–623 (2011).

47. Darieva, Z. *et al.* Cell cycle-regulated transcription through the FHA domain of Fkh2p and the coactivator Ndd1p. *Curr Biol* **13**, 1740–1745 (2003).

48. Enserink, J. M. & Kolodner, R. D. An overview of Cdk1-controlled targets and processes. *Cell Div* **5**, 11 (2010).

49. Zhu, G. *et al.* Two yeast forkhead genes regulate the cell cycle and pseudohyphal growth. *Nature* **406**, 90–94 (2000).

50. Spellman, P. T. *et al.* Comprehensive Identification of Cell Cycle–regulated Genes of the Yeast Saccharomyces cerevisiae by Microarray Hybridization. *Mol Biol Cell* **9**, 3273–3297 (1998).

51. Rahal, R. & Amon, A. Mitotic CDKs control the metaphase-anaphase transition and trigger spindle elongation. *Genes & development* **22**, 1534–48 (2008).

52. Machu, C. *et al.* Spatially distinct functions of Clb2 in the DNA damage response. *Cell Cycle* **13**, 383–398 (2014).

53. Veis, J., Klug, H., Koranda, M. & Ammerer, G. Activation of the G2/M-specific gene CLB2 requires multiple cell cycle signals. *Molecular and cellular biology* **27**, 8364–73 (2007).

54. Maher, M., Cong, F., Kindelberger, D., Nasmyth, K. & Dalton, S. Cell cycle-regulated transcription of the CLB2 gene is dependent on Mcm1 and a ternary complex factor. *Mol Cell Biol* **15**, 3129–3137 (1995).

55. Trcek, T., Larson, D. R., Moldon, A., Query, C. C. & Singer, R. H. Single-Molecule mRNA Decay Measurements Reveal Promoter-Regulated mRNA Stability in Yeast. *Cell* **147**, 1484–1497 (2011).

56. Visintin, R. & Amon, A. Regulation of the mitotic exit protein kinases Cdc15 and Dbf2. *Molecular biology of the cell* **12**, 2961–74 (2001).

57. Hotz, M. & Barral, Y. The Mitotic Exit Network: new turns on old pathways. *Trends in Cell Biology* **24**, 145–152 (2014).

58. Femino, A. M., Fay, F. S., Fogarty, K. & Singer, R. H. Visualization of single RNA transcripts in situ. *Science* **280**, 585–90 (1998).

59. Raj, A., van den Bogaard, P., Rifkin, S. A., van Oudenaarden, A. & Tyagi, S. Imaging individual mRNA molecules using multiple singly labeled probes. *Nat Methods* **5**, 877–9 (2008).

60. Eliscovich, C., Shenoy, S. M. & Singer, R. H. Imaging mRNA and protein interactions within neurons. *Proceedings of the National Academy of Sciences of the United States of America* **114**, E1875–E1884 (2017).

61. Wu, B., Eliscovich, C., Yoon, Y. J. & Singer, R. H. Translation dynamics of single mRNAs in live cells and neurons. *Science* **352**, 1430–5 (2016).

62. Tutucci, E. & Singer, R. H. Simultaneous Detection of mRNA and Protein in S. Cerevisiae by Single Molecule FISH and Immunofluorescence. *Methods in Molecular Biology*.

63. Wu, B. *et al.* Synonymous modification results in high-fidelity gene expression of repetitive protein and nucleotide sequences. *Genes & development* **29**, 876–86 (2015).

64. Tutucci, E., Maekiniemi, A. & Singer, R. H. Single molecule mRNA Fluorescent In Situ Hybridization combined to Immunofluorescence in S. cerevisiae: Dataset and quantification. *Mendeley repository* doi:http://dx.doi.org/10.17632/bcmn9cxyzs.2.

65. Tutucci, E., Livingston, N. M., Singer, R. H. & Wu, B. Imaging mRNA in vivo, from Birth to Death. *Annu Rev Biophys* **47**, (2018).

66. Vera, M., Biswas, J., Senecal, A., Singer, R. H. & Park, H. Y. Single-Cell and Single-Molecule Analysis of Gene Expression Regulation. *Annu Rev Genet* **50**, 267–291 (2016).

67. Tutucci, E. *et al.* An improved MS2 system for accurate reporting of the mRNA life cycle. *Nat Methods* **15**, 81–89 (2018).

68. Tutucci, E., Vera, M. & Singer, R. H. Single-mRNA detection in living S. cerevisiae using a re-engineered MS2 system. *Nat Protoc* **13**, 2268–2296 (2018).

69. Pichon X, Robert MC, Bertrand E, Singer RH, & Tutucci E. New generations of MS2 variants and MCP fusions to detect single mRNAs in living eukaryotic cells. **Methods in Molecular Biology**, (In Press).

70. Maekiniemi, A., Singer, R. H. & Tutucci, E. Single molecule mRNA fluorescent in situ hybridization combined with immunofluorescence in S. cerevisiae: Dataset and quantification. *Data in Brief* **30**, 105511 (2020).

71. Tutucci, E. & Singer, R. H. Simultaneous Detection of mRNA and Protein in S. cerevisiae by Single-Molecule FISH and Immunofluorescence. *Methods Mol. Biol.* **2166**, 51–69 (2020).

72. Taberner, F. J., Quilis, I. & Igual, J. C. Spatial regulation of the Start repressor Whi5. *Cell Cycle* **8**, 3013–3022 (2009).

73. Kilmartin, J. V. & Adams, A. E. Structural rearrangements of tubulin and actin during the cell cycle of the yeast Saccharomyces. *J Cell Biol* **98**, 922–933 (1984).

74. Zenklusen, D., Larson, D. R. & Singer, R. H. Single-RNA counting reveals alternative modes of gene expression in yeast. *Nat Struct Mol Biol* **15**, 1263–71 (2008).

75. Sanchez, A. & Golding, I. Genetic determinants and cellular constraints in noisy gene expression. *Science* **342**, 1188–93 (2013).

76. Pichon, X., Robert, M.-C., Bertrand, E., Singer, R. H. & Tutucci, E. New Generations of MS2 Variants and MCP Fusions to Detect Single mRNAs in Living Eukaryotic Cells. *Methods Mol. Biol.* **2166**, 121–144 (2020).

77. Haimovich, G. *et al.* Use of the MS2 aptamer and coat protein for RNA localization in yeast: A response to 'MS2 coat proteins bound to yeast mRNAs block 5' to 3' degradation and trap mRNA decay products: implications for the localization of mRNAs by MS2-MCP system'. *RNA* **22**, 660–6 (2016).

78. Garcia, J. F. & Parker, R. MS2 coat proteins bound to yeast mRNAs block 5' to 3' degradation and trap mRNA decay products: implications for the localization of mRNAs by MS2-MCP system. *RNA* **21**, 1393–5 (2015).

79. Schlichting, J. K. Modeling synchronization effects in the yeast cell cycle. (2019) doi:http://dx.doi.org/10.18452/19835.

80. Amoussouvi, A. *et al.* Transcriptional timing and noise of yeast cell cycle regulators—a single cell and single molecule approach. *npj Systems Biology and Applications* **4**, 1–10 (2018).

81. Johnston, G. C., Pringle, J. R. & Hartwell, L. H. Coordination of growth with cell division in the yeast Saccharomyces cerevisiae. *Experimental cell research* **105**, 79–98 (1977).

82. Leitao, R. M. & Kellogg, D. R. The duration of mitosis and daughter cell size are modulated by nutrients in budding yeast. *J Cell Biol* **216**, 3463–3470 (2017).

83. Park, H. Y. *et al.* Visualization of dynamics of single endogenous mRNA labeled in live mouse. *Science* **343**, 422–4 (2014).

84. Edelmann, F. T. *et al.* Molecular architecture and dynamics of ASH1 mRNA recognition by its mRNA-transport complex. *Nature Structural & Molecular Biology* **24**, 152–161 (2017).

85. Chartrand, P., Meng, X.-H., Singer, R. H. & Long, R. M. Structural elements required for the localization of ASH1 mRNA and of a green fluorescent protein reporter particle in vivo. *Current Biology* **9**, 333–338 (1999).

86. Gonzalez, I., Buonomo, S. B. C., Nasmyth, K. & Ahsen, U. von. ASH1 mRNA localization in yeast involves multiple secondary structural elementsand Ash1 protein translation. *Current Biology* **9**, 337–340 (1999).

87. Stueland, M., Wang, T., Park, H. Y. & Mili, S. RDI Calculator: An Analysis Tool to Assess RNA Distributions in Cells. *Sci Rep* **9**, 1–10 (2019).

88. Moissoglu, K., Yasuda, K., Wang, T., Chrisafis, G. & Mili, S. Translational regulation of protrusion-localized RNAs involves silencing and clustering after transport. *eLife* **8**,.

89. Cormack, B. P. *et al.* Yeast-enhanced green fluorescent protein (yEGFP): a reporter of gene expression in Candida albicans. *Microbiology (Reading)* **143 (Pt 2)**, 303–311 (1997).

90. Arava, Y. *et al.* Genome-wide analysis of mRNA translation profiles in Saccharomyces cerevisiae. *Proc Natl Acad Sci U S A* **100**, 3889–3894 (2003).

91. Katz, Z. B. *et al.* Mapping translation 'hot-spots' in live cells by tracking single molecules of mRNA and ribosomes. *Elife* **5**, (2016).

92. Biswas, J., Liu, Y., Singer, R. H. & Wu, B. Fluorescence Imaging Methods to Investigate Translation in Single Cells. *Cold Spring Harb Perspect Biol* **11**, (2019).

93. Turner, J. J., Ewald, J. C. & Skotheim, J. M. Cell Size Control in Yeast. *Current Biology* **22**, R350–R359 (2012).

94. Groisman, I. *et al.* CPEB, maskin, and cyclin B1 mRNA at the mitotic apparatus: implications for local translational control of cell division. *Cell* **103**, 435–447 (2000).

95. Yasuda, K., Kotani, T. & Yamashita, M. A cis-acting element in the coding region of cyclin B1 mRNA couples subcellular localization to translational timing. *Developmental Biology* **382**, 517–529 (2013).

96. Kotani, T., Yasuda, K., Ota, R. & Yamashita, M. Cyclin B1 mRNA translation is temporally controlled through formation and disassembly of RNA granules. *J Cell Biol* **202**, 1041–1055 (2013).

97. Spiesser, T. W., Kühn, C., Krantz, M. & Klipp, E. Bud-Localization of CLB2 mRNA Can Constitute a Growth Rate Dependent Daughter Sizer. *PLOS Computational Biology* **11**, e1004223 (2015).

98. Mueller, F. *et al.* FISH-quant: automatic counting of transcripts in 3D FISH images. *Nat Methods* **10**, 277–8 (2013).

99. Kamenova, I. *et al.* Co-translational assembly of mammalian nuclear multisubunit complexes. *Nat Commun* **10**, 1740 (2019).

100. Olivier, C. *et al.* Identification of a conserved RNA motif essential for She2p recognition and mRNA localization to the yeast bud. *Mol Cell Biol* **25**, 4752–66 (2005).

101. Lorenz, R. *et al.* ViennaRNA Package 2.0. *Algorithms Mol Biol* **6**, 26 (2011).

102. Lorenz, R., Hofacker, I. L. & Stadler, P. F. RNA folding with hard and soft constraints. *Algorithms Mol Biol* **11**, 8 (2016).

103. Darty, K., Denise, A. & Ponty, Y. VARNA: Interactive drawing and editing of the RNA secondary structure. *Bioinformatics* **25**, 1974–1975 (2009).

104. Bivand, R. S., Pebesma, E. & Gómez-Rubio, V. *Applied Spatial Data Analysis with R*. (Springer-Verlag, 2013). doi:10.1007/978-1-4614-7618-4.

105. Sprouffske, K. & Wagner, A. Growthcurver: an R package for obtaining interpretable metrics from microbial growth curves. *BMC Bioinformatics* **17**, 172 (2016).

106. Wickham, H. *ggplot2: Elegant Graphics for Data Analysis*. (Springer International Publishing, 2016). doi:10.1007/978-3-319-24277-4.

107. Wickham, H. *et al.* Welcome to the Tidyverse. *Journal of Open Source Software* **4**, 1686 (2019).

108. RColorBrewer: ColorBrewer Palettes version 1.1-2 from CRAN. https://rdrr.io/cran/RColorBrewer/.

109. dplyr: A Grammar of Data Manipulation — dplyr-package. https://dplyr.tidyverse.org/reference/dplyr-package.html.

110. Benaglia, T., Chauveau, D., Hunter, D. R. & Young, D. S. mixtools: An R Package for Analyzing Mixture Models. *Journal of Statistical Software* **32**, 1–29 (2010).

111. Costanzo, M. *et al.* CDK Activity Antagonizes Whi5, an Inhibitor of G1/S Transcription in Yeast. *Cell* **117**, 899–913 (2004).

112. Wagner, M. V. *et al.* Whi5 regulation by site specific CDK-phosphorylation in Saccharomyces cerevisiae. *PLoS ONE* **4**, e4300 (2009).

Figure 1

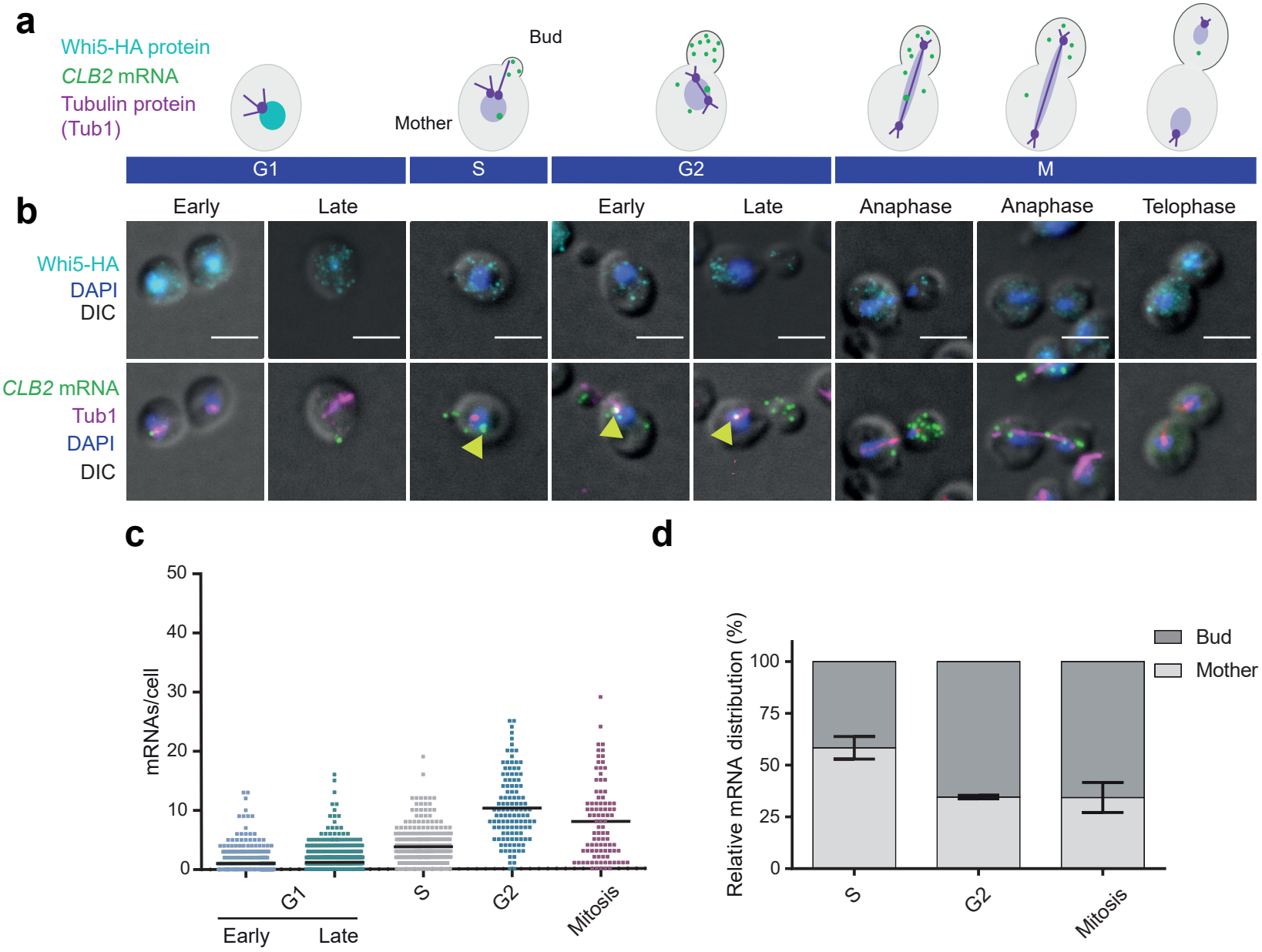
a
Whi5-HA protein
CLB2 mRNA
Tubulin protein (Tub1)
Bud
Mother
G1
S
G2
M
b
Early
Late
Early
Late
Anaphase
Anaphase
Telophase
Whi5-HA
DAPI
DIC
CLB2 mRNA
Tub1
DAPI
DIC
c
mRNAs/cell
50
40
30
20
10
0
G1
S
G2
Mitosis
Early
Late
d
Relative mRNA distribution (%)
100
75
50
25
0
Bud
Mother
S
G2
Mitosis

Figure 1S

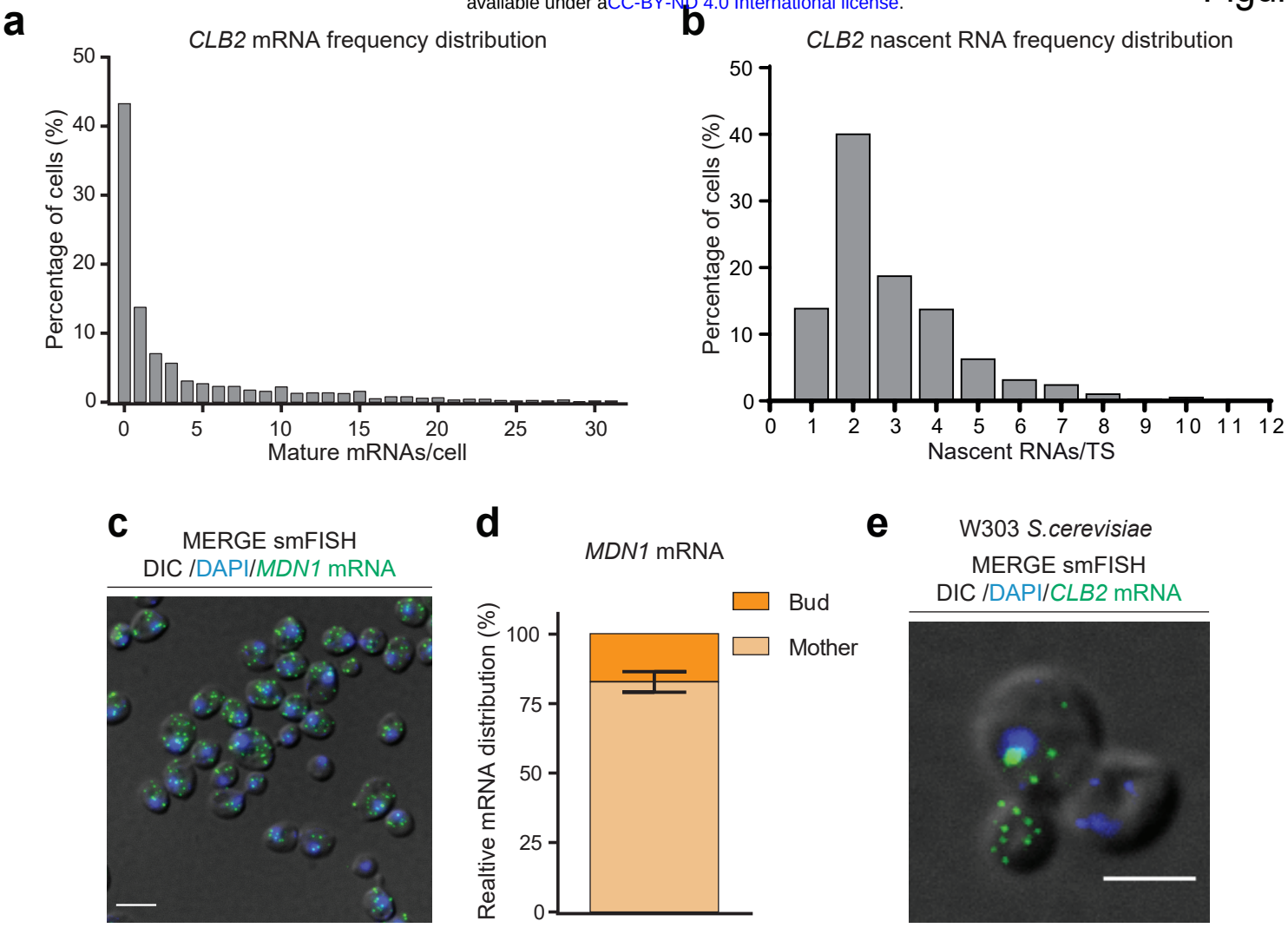

Figure 2

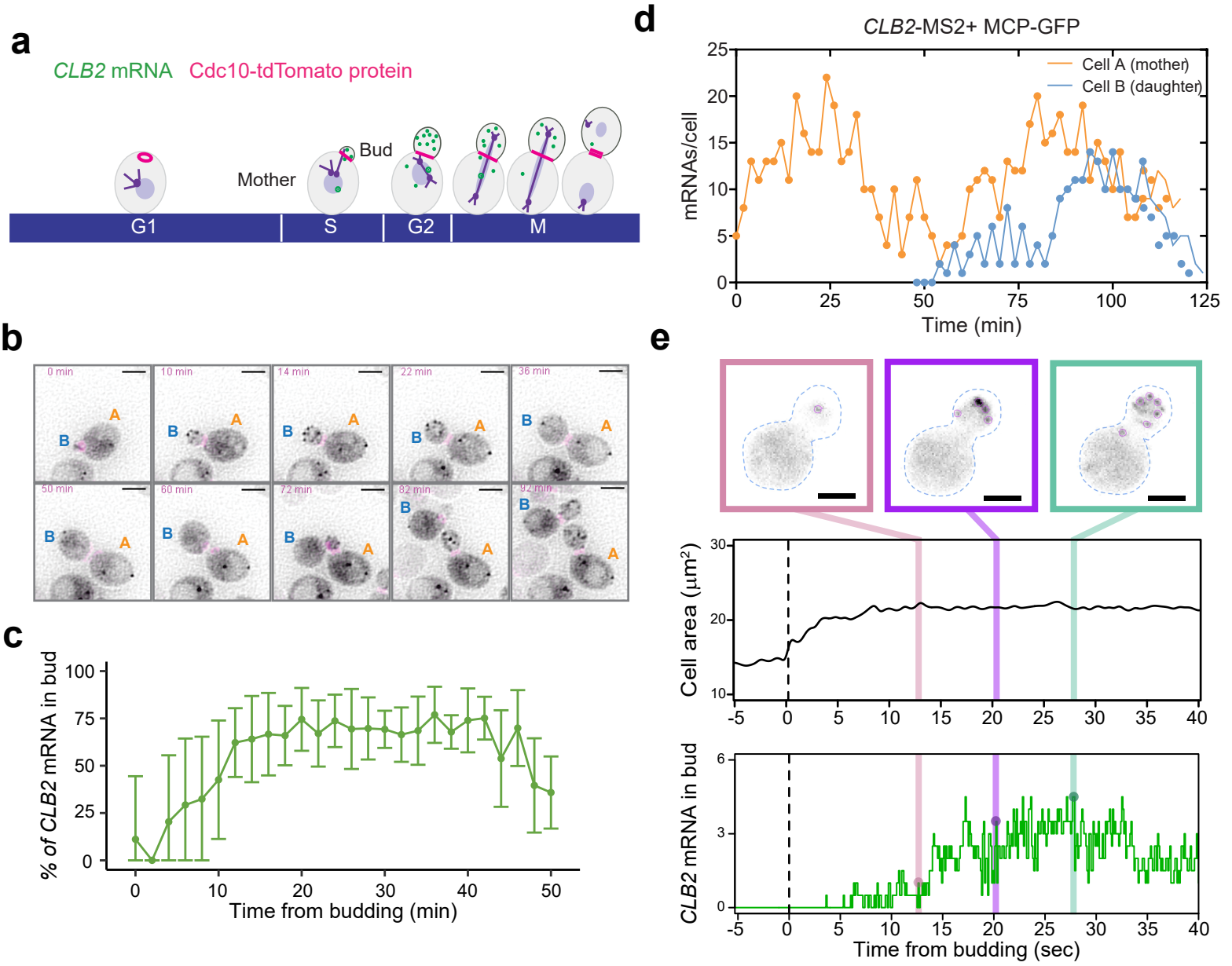

Figure 2S

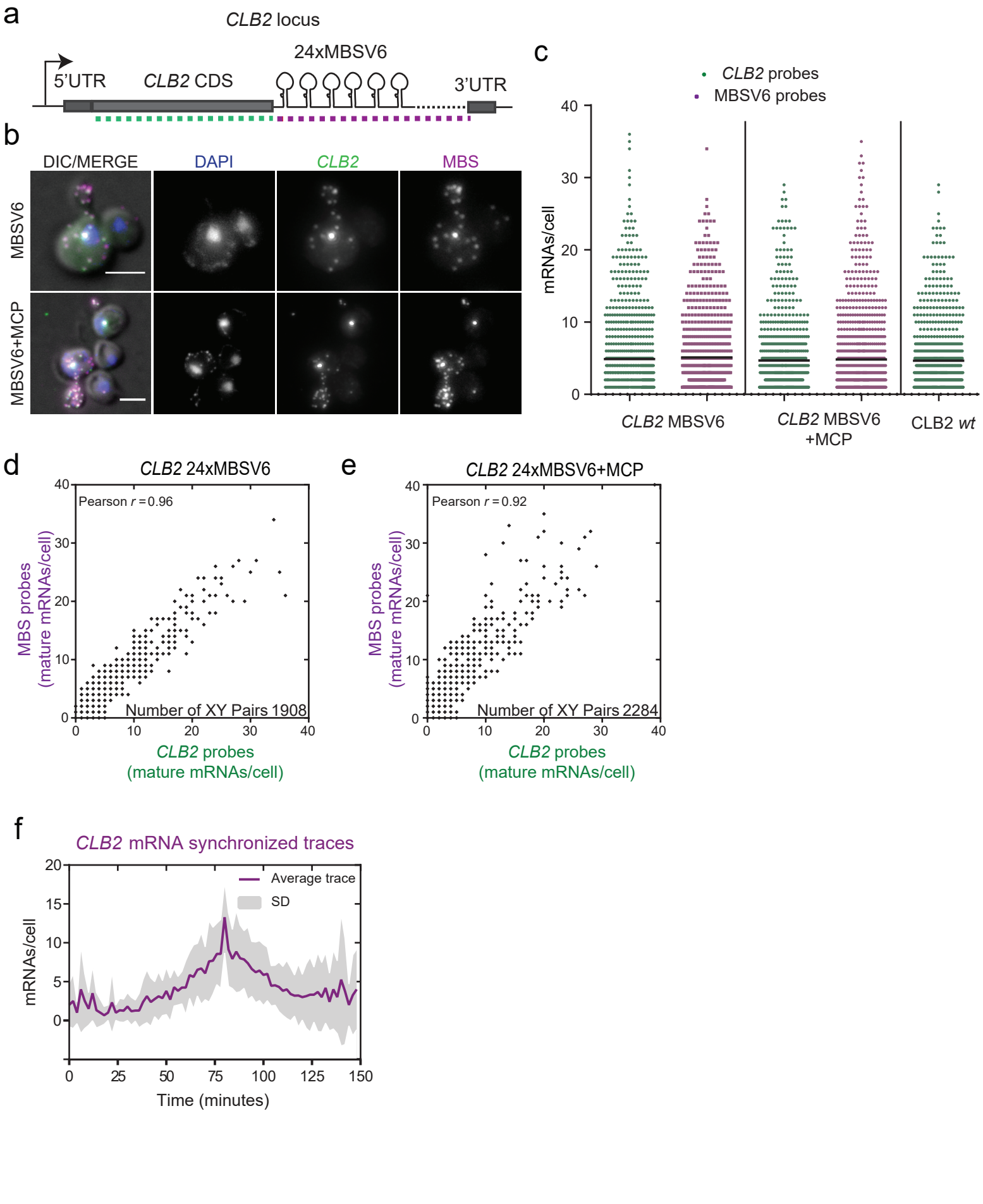

Figure 3

a

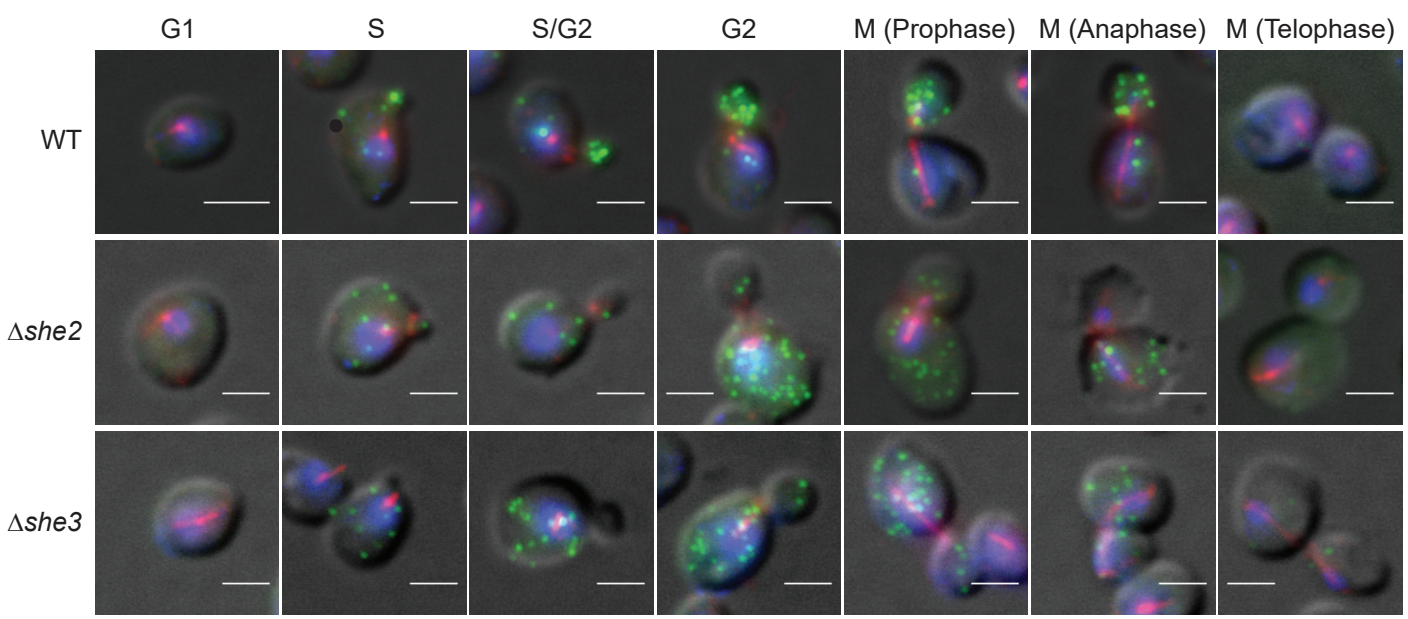

b

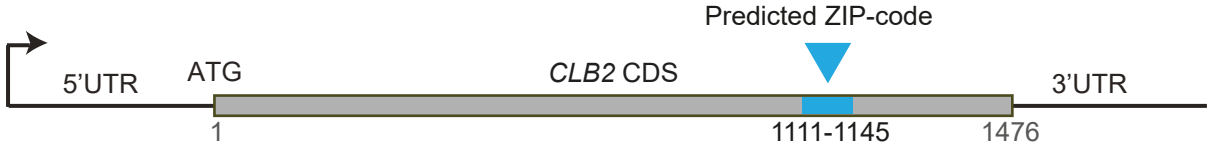

c

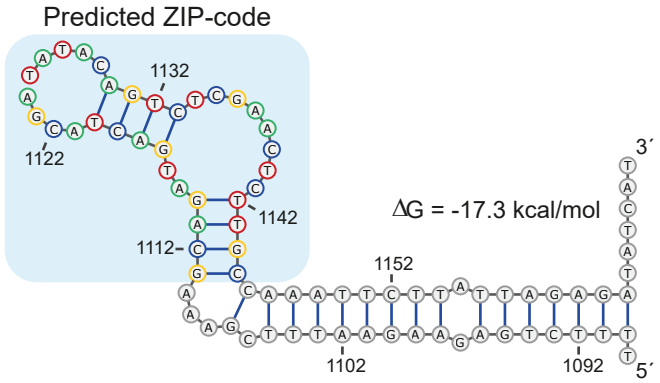

d

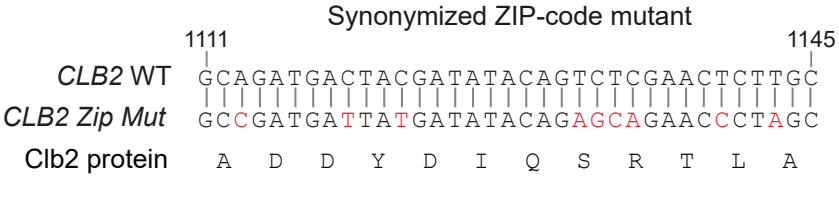

e

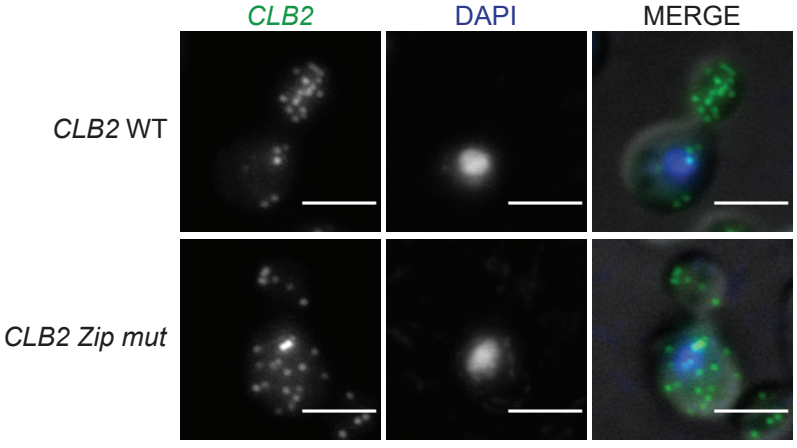

f

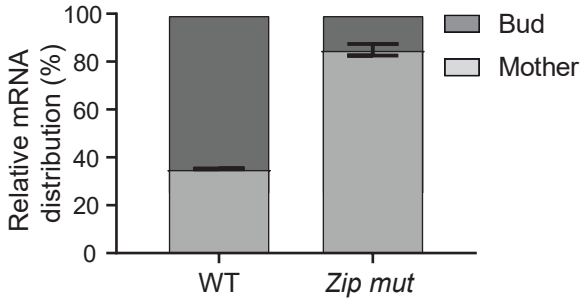

g

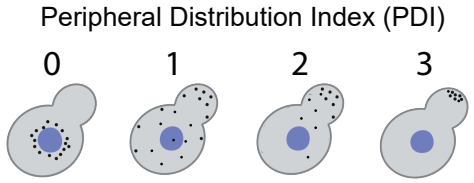

h

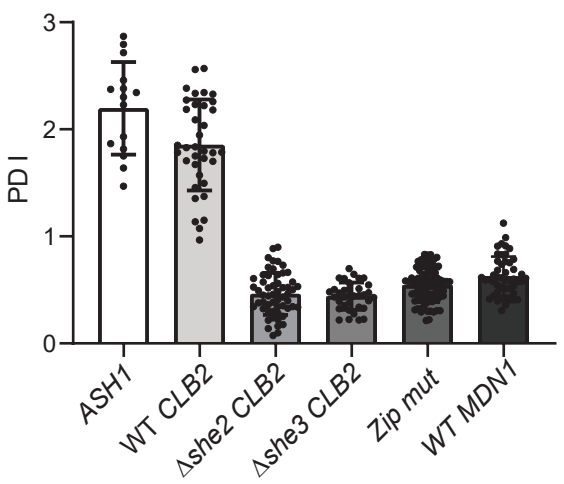

Figure 3S

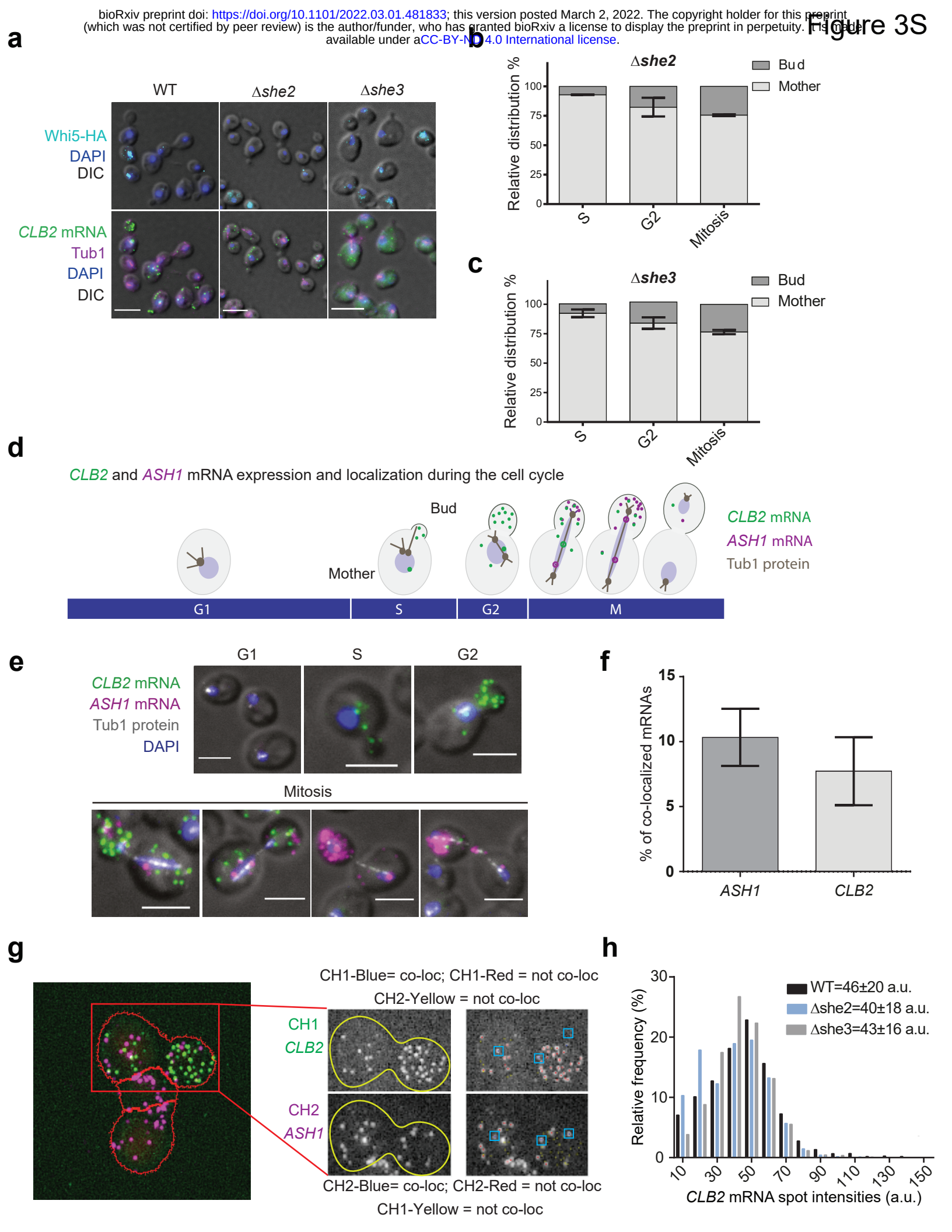

Figure 4

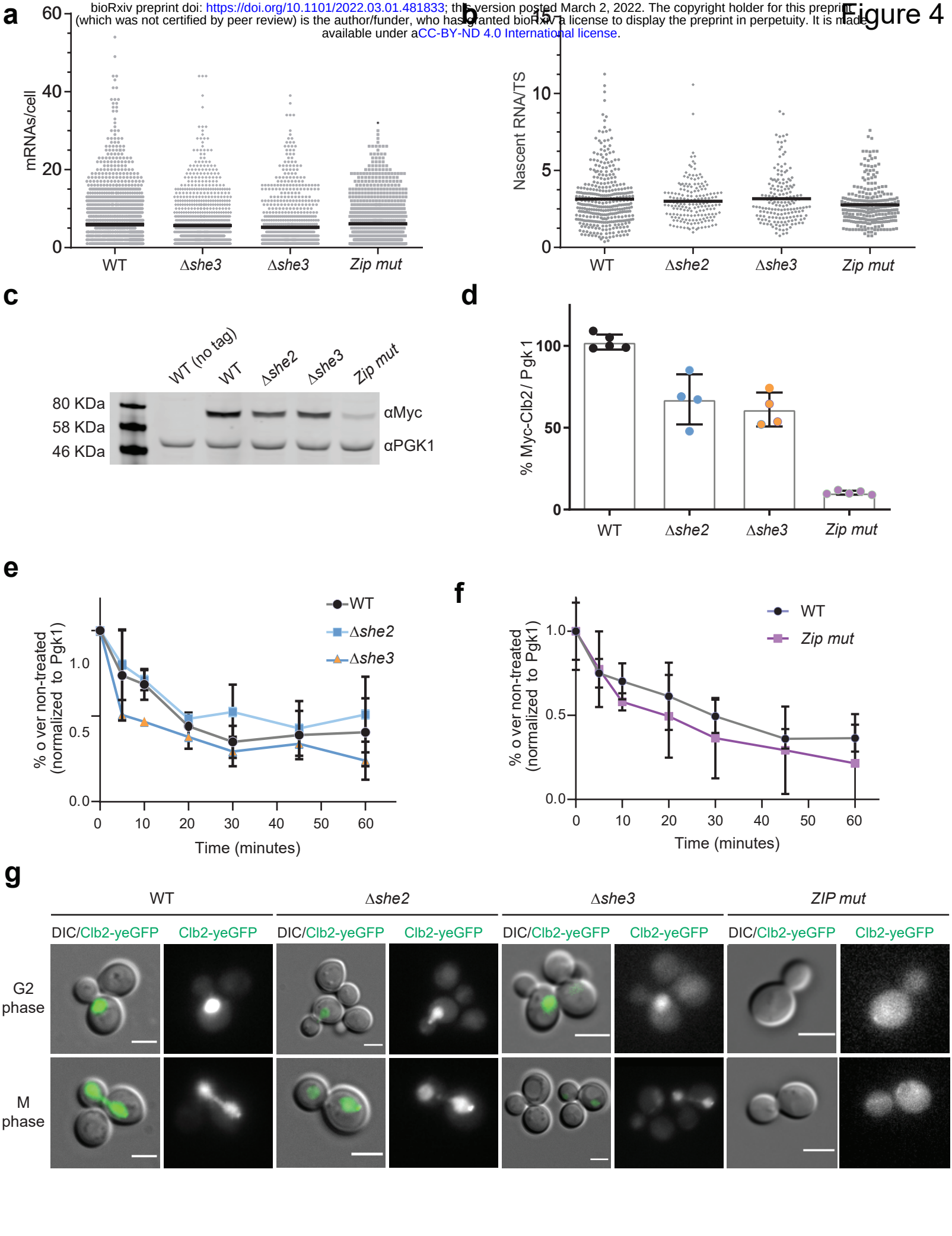

Figure 4S

a

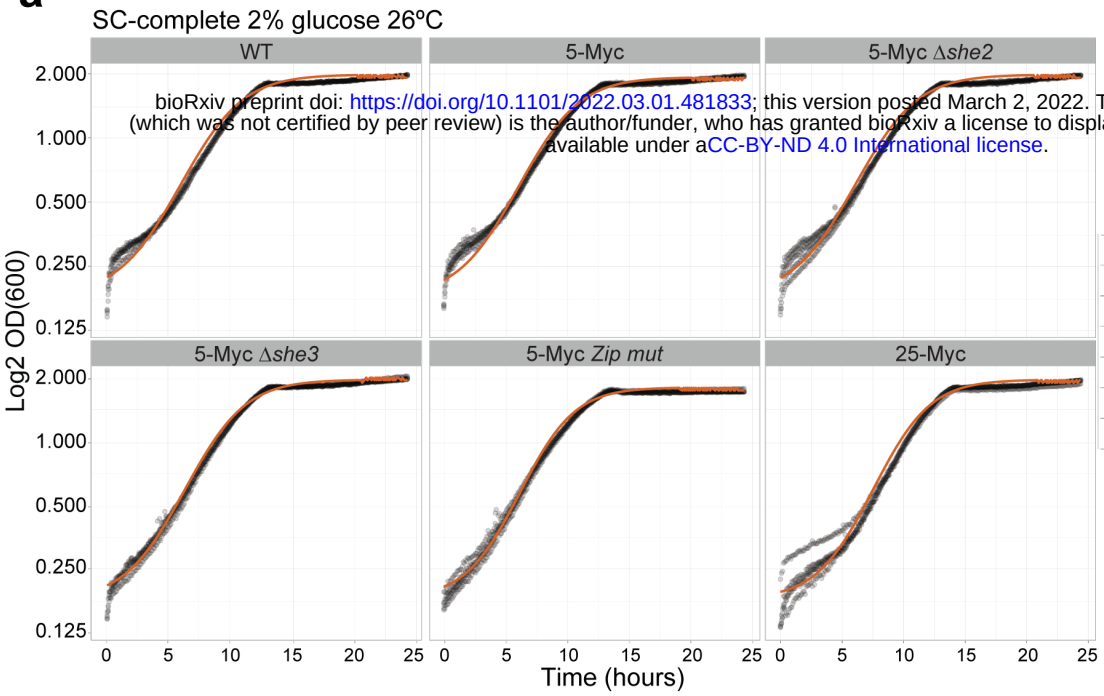

	K (yield)	r (growth rate)
WT	1.78	0.44
5Myc	1.75	0.45
5Myc-Δshe2	1.77	0.44
5Myc-Δshe3	1.78	0.45
5Myc-*ZIP mut*	1.59	0.49
25Myc	1.75	0.48

b

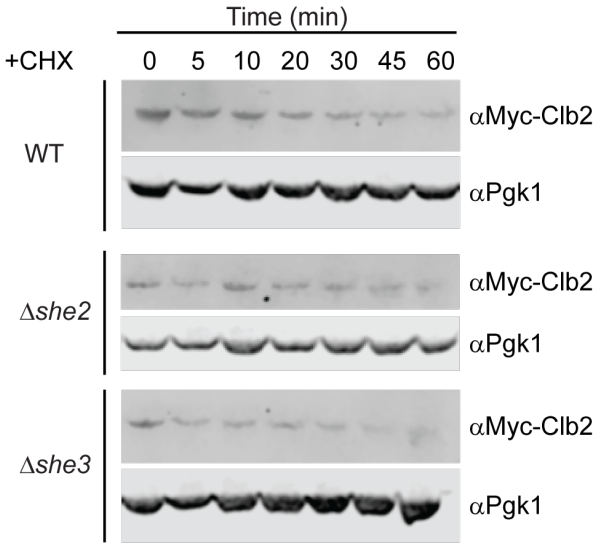

c

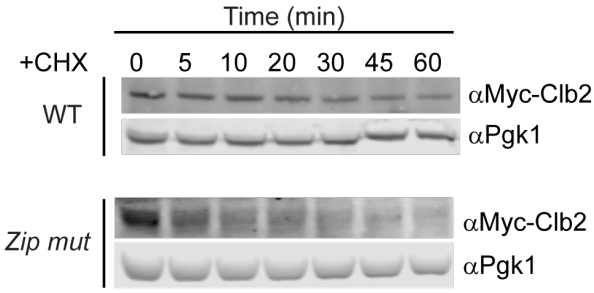

d

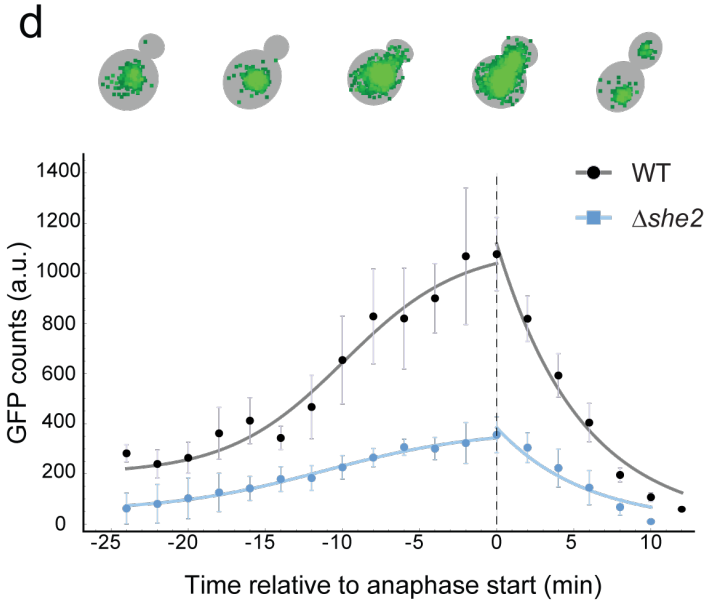

e

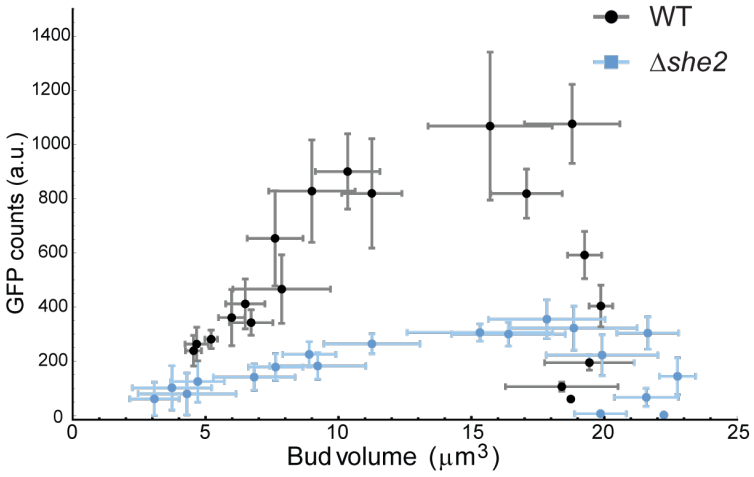

Figure 5

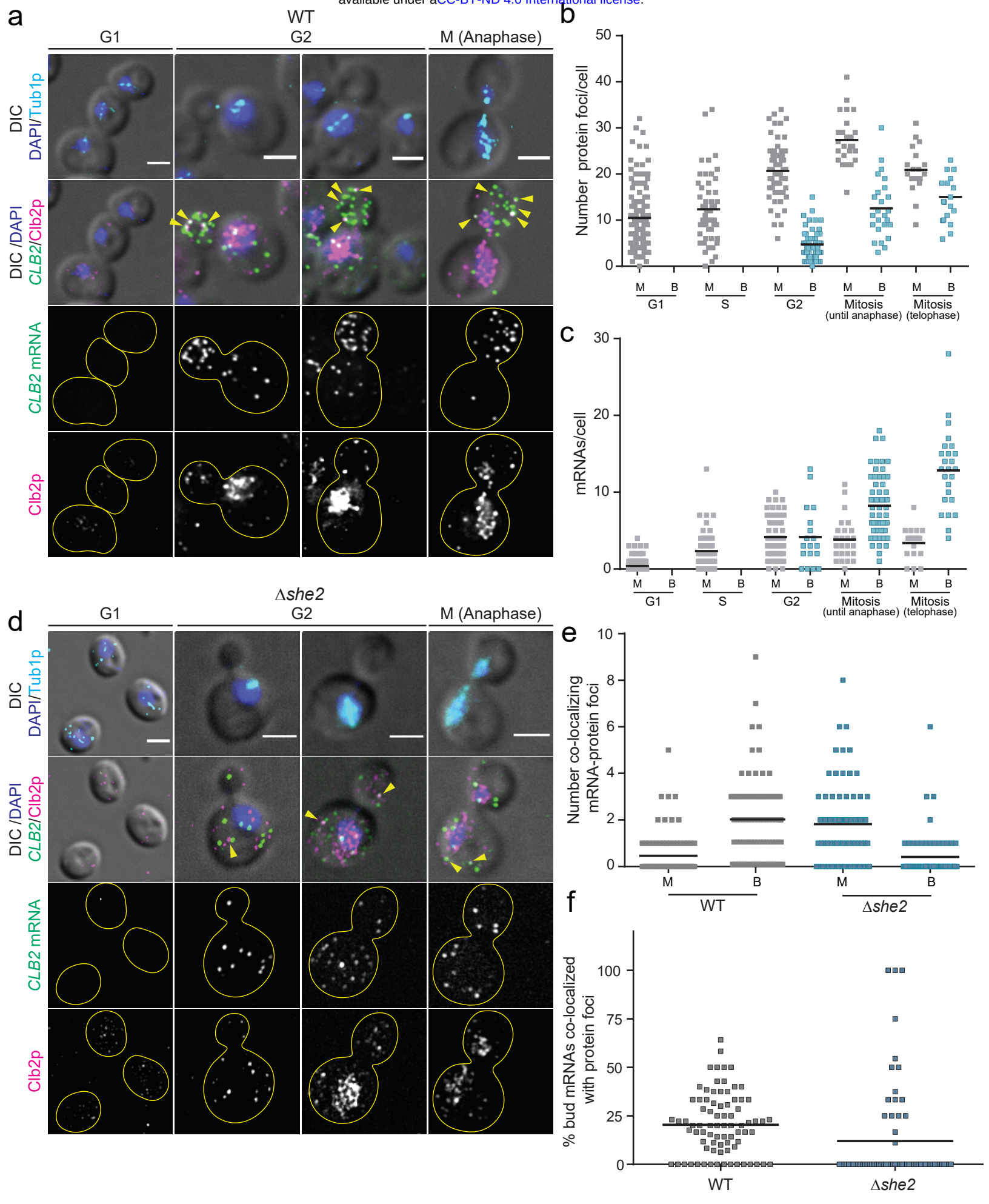

Figure 5S

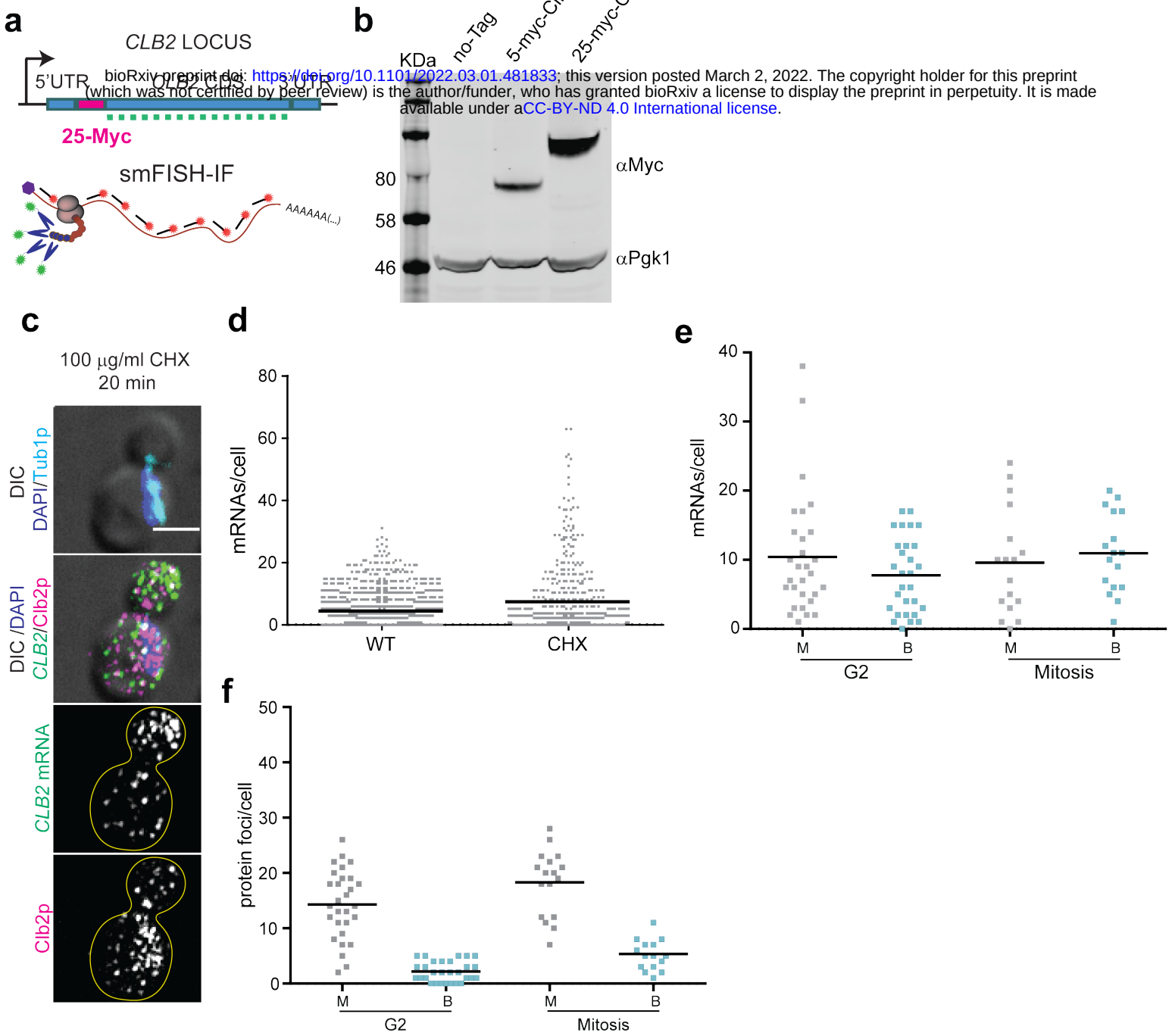

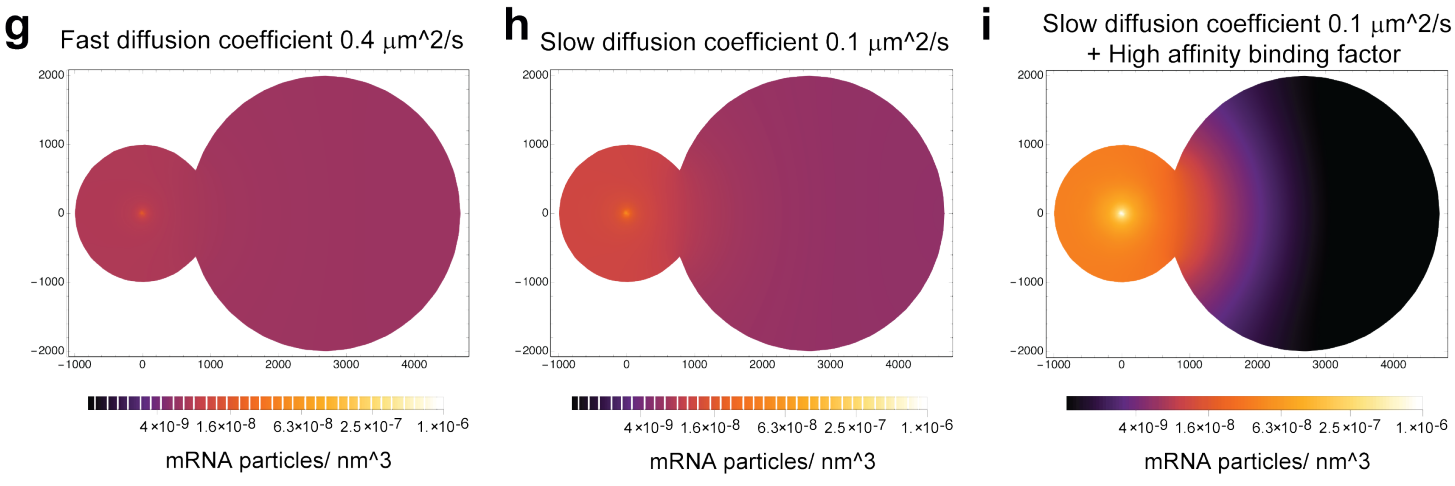

Figure 6

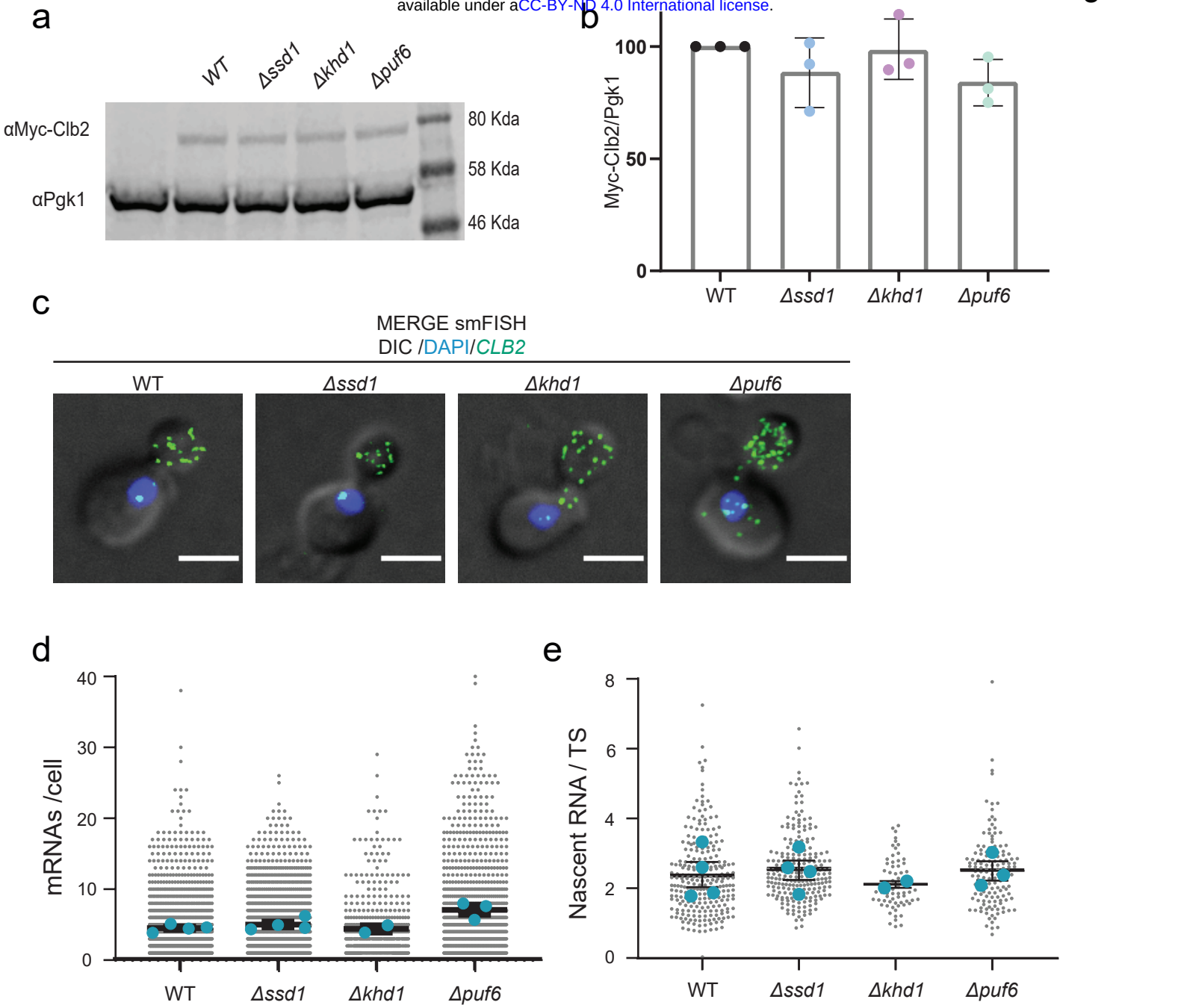

Figure 6S

a

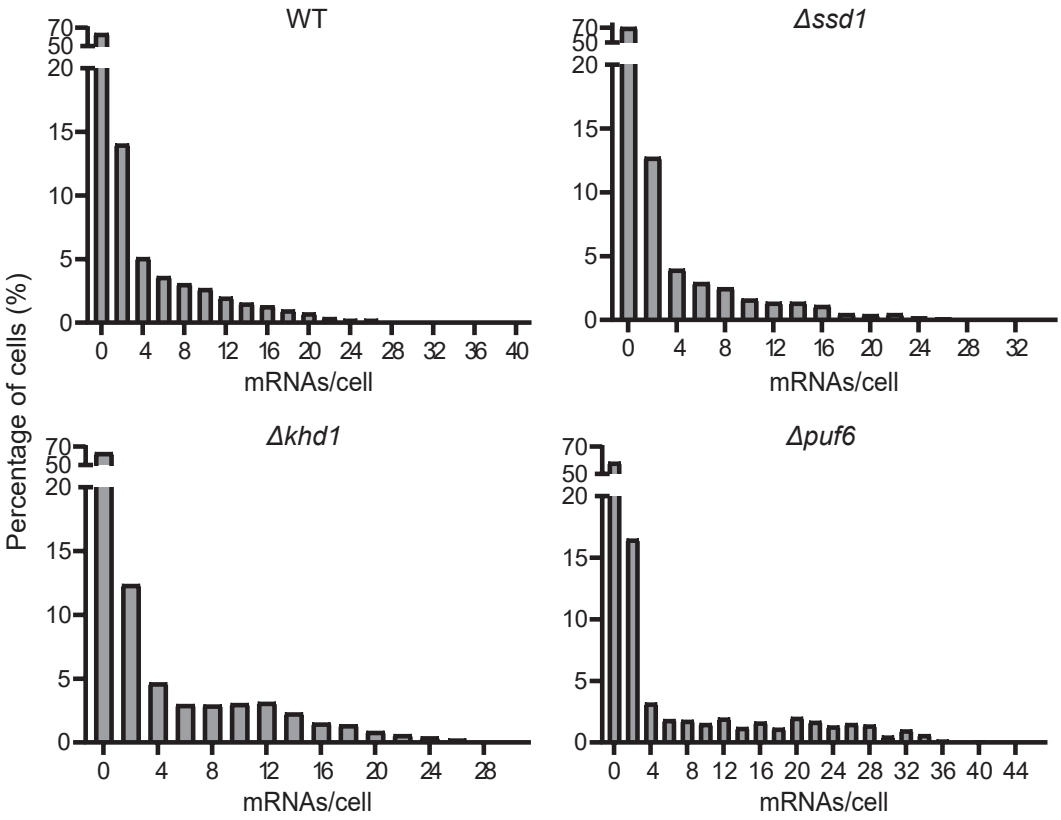

b

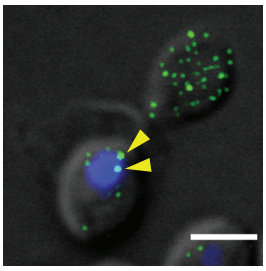

c

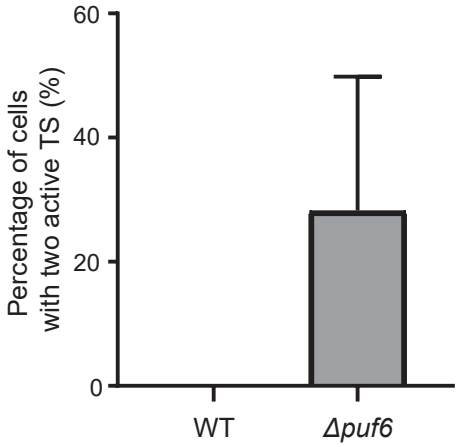

Figure 7

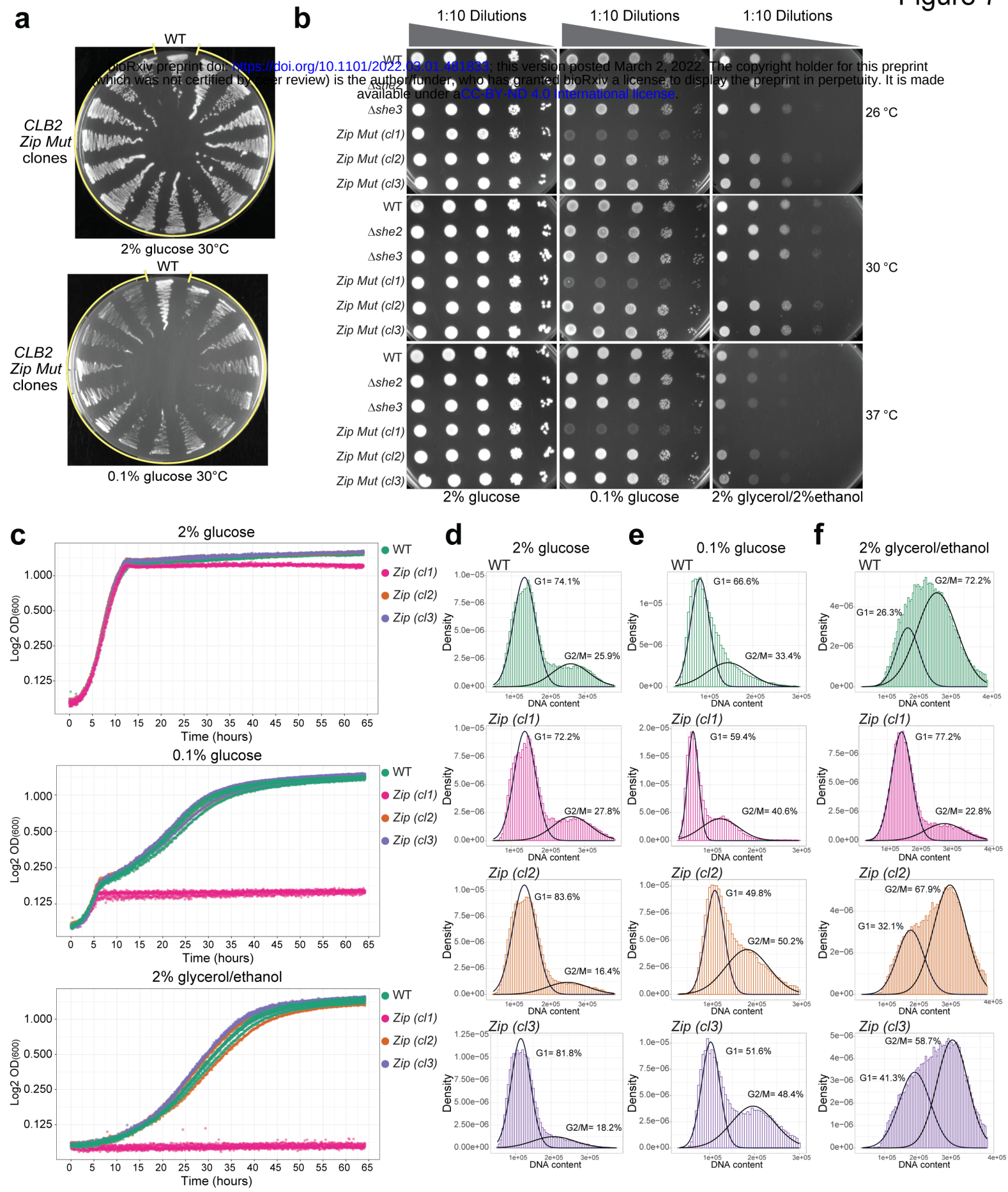

Figure 7S